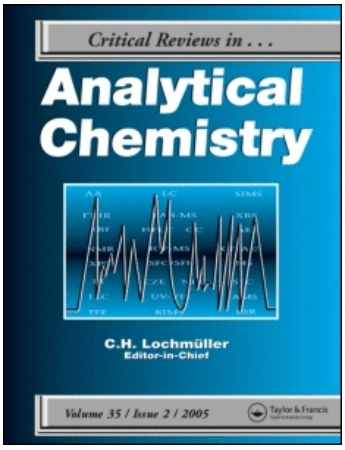

Critical Reviews in Analytical Chemistry
Publication details, including instructions for authors and subscription information:
http://www.informaworld.com/smpp/title~content=t713400837

Proton Induced X-Ray Emission Analysis: Part I

Khan Md. Rashiduzzaman; Dennis Crumpton; Sven Johansson

To cite this Article Rashiduzzaman, Khan Md. , Crumpton, Dennis and Johansson, Sven(1981) 'Proton Induced X-Ray Emission Analysis: Part I', Critical Reviews in Analytical Chemistry, 11: 2, 103 — 160
To link to this Article: DOI: 10.1080/10408348108542708
URL: http://dx.doi.org/10.1080/10408348108542708

PROTON INDUCED X-RAY EMISSION ANALYSIS: PART I*

Authors: **Md. Rashiduzzaman Khan**
Atomic Energy Organization
Nuclear Research Centre
Tehran, Iran

Dennis Crumpton
Physics Department
University of Aston
Birmingham, England

Referee: Sven Johansson
Department of Nuclear Physics
Lund Institute of Technology
Lund, Sweden

TABLE OF CONTENTS

* Based in part on an earlier review by M. R. Khan. Atomic Energy Organization of Iran. Technical Report AEOI-58, NRC-76-37, 1976.

I. INTRODUCTION

If electrons are removed from the inner shells of atoms the vacancies created are filled by electrons from higher energy levels, giving rise to the emission of radiation. For all but the lightest elements this emission is in the X-ray region of the electromagnetic spectrum. The energy of the emitted X-ray is characteristic of the element emitting the radiation and hence its observation forms a method of identification. The initial inner-shell ionization of the atom can be initiated by bombarding the sample under investigation with photons, electrons, or heavier charged particles, such as alpha particles or protons, giving rise to a variety of microanalytical techniques; X-ray fluorescence analysis, electron microprobe analysis, alpha particle and proton-induced X-ray emission analysis.

Currently there is considerable interest in microanalysis based on proton-induced X-ray emission (PIXE). This interest has been brought about by the general worldwide availability of particle accelerators of 1 to 3 MeV, the introduction of high resolution lithium-drifted silicon detectors, the development of small on-line computers, and not least, by the many desirable features offered by proton-induced X-ray emission analysis itself. Such features include:

1. Multielemental analysis in a single run.
2. Low bremsstrahlung radiation background leading to a high signal-to-noise ratio.
3. High sensitivity for all elements with atomic number greater than 11.
4. Under interference-free conditions the sensitivity does not vary markedly from one element to the next.
5. Ideally suited to very small samples.
6. Relatively short analysis times.
7. Can be employed nondestructively.
8. A high degree of automation possible. This is particularly important in many studies involving large numbers of routine analyses, such as environmental and biological investigations.

The emergence of proton-induced X-ray emission analysis as a major technique for multielemental trace analysis has stimulated interest in understanding the interaction phenomenon between an incident-charged particle and the inner-shell electrons, in the presence of the nuclear Coulomb field. Testing the assumptions involved in the different theories and making comparisons between theories is achieved by detailed studies of the inner-shell ionization cross-sections. Such studies often result in modifications or new approaches to the theories.

The tremendous potential that proton-induced X-ray emission analysis possesses as an analytical tool was first demonstrated in 1970 by Johansson et al.[1] for protons of 3 MeV. Under favorable conditions, Johansson et al.[1,2] found that they were able to detect quantities down to 10^{-11} to 10^{-13} g for elements with atomic numbers in the range 15 to 92. With improvements in measuring techniques they predicted that the minimum detectable limit (MDL) for these elements would be of the order of 10^{-15} g. The present MDL is already an order or two better than other analytical techniques. Detailed comparisons of the analytical capabilities of PIXE compared with other analytical techniques (α particle-induced X-ray analysis, X-ray fluorescence analysis, electron microprobe analysis, neutron activation analysis, etc.), have been made by a number of authors including Duggan et al.,[3] Folkmann et al.,[4] Cooper,[5] Perry and Brady,[6] Reuter and Lurio,[7] and Ahlberg and Adams.[8] These techniques should be regarded as complementary since one may be more appropriate than another under specific conditions. For example, neutron activation analysis gives good sensitivity for some elements with $Z < 11$, a region not

accessible to PIXE. Lead, on the other hand, which is of major concern in environmental pollution studies, cannot be examined by activation methods but can be detected with high sensitivity using PIXE analysis.

Although when compared with competing methods PIXE exhibits the highest sensitivity over the widest possible range of the periodic table, it also has its limitations, many of which have been discussed by Verba et al.[9] Problems relating to the backing materials used to support samples, sample preparation, and data analysis have been discussed in the many early papers on analysis published by Johansson et al.,[1,2] Mangelson et al.,[10] Jolly and White,[11] Flocchini et al.,[12] Walter et al.,[13] Valkovic,[14] Thomas et al.[15] and Barns et al.[16] At present, the limiting factors in PIXE analysis arise from problems associated with the backing material, in terms of its purity, conductivity, and strength; the detectors, in terms of resolution, efficiency at low energies, and count-rate capability; and the background associated with the measurements. In addition, the present techniques for sample preparations, particularly for fibrous tissue, are inadequate. Although several authors, including Reuter et al.,[17] Ahlberg,[18] Pabst,[19,20] Feldman et al.,[21] Van der Kam et al.,[22] Lin et al.,[23] and Huda,[24] have studied the complex situation relating to thick targets, present techniques are not entirely satisfactory.

The growing worldwide concern with pollution and the translocation of pollutants through the ecosystem requires the accurate determination of trace elements in, for example, biological, pathological, metallurgical, and environmental samples, and hence the demand for a quick, efficient routine analysis system of high sensitivity is continuously increasing. With superior sensitivity, simultaneous multielemental capability and reasonably easy data handling procedures, PIXE is responding to this need and is rapidly becoming established as a major analytical technique. This is clearly borne out by the significant number of recent publications on the topic and by the fact that many international conferences[25-27] now include sessions in their programs on PIXE analysis. The first International Conference on Particle Induced X-ray Emission and its Analytical Applications was held in Lund, Sweden in 1976, the Proceedings[28] of which are a valuable source of information on the topic. A number of important review articles have also been published which include those of Valkovic,[14] Folkmann,[29] Deconninck et al.,[30] and Johansson and Johansson.[31] More recently, reviews of the PIXE analysis work at specific institutions have been published, including those of Wilk et al.,[32] Van der Heide et al.,[33] and Akselsson and Johansson.[34]

II. PRODUCTION OF X-RAYS BY CHARGED PARTICLES

When an energetic particle passes through matter it loses most of its energy through interaction with atomic electrons producing excitation and ionization. The maximum energy, T_m, that can be transferred by a heavy particle, mass M, energy E, to a free electron, mass m, is given by

$$T_m = \frac{4Mm}{(m + M)^2} \cdot E \qquad (1)$$

For protons $T_m \simeq E/460$, which for protons of energy 1 to 3 MeV gives electrons of energy of approximately 2 to 6 keV, a point we shall return to later. There is also an appreciable probability that an inelastic collision with the atom as a whole will take place, releasing a bound electron from an inner shell of the atom. This inner-shell ionization thus creates a vacancy which is filled as the atom de-excites. A number of possibilities exist for the de-excitation.

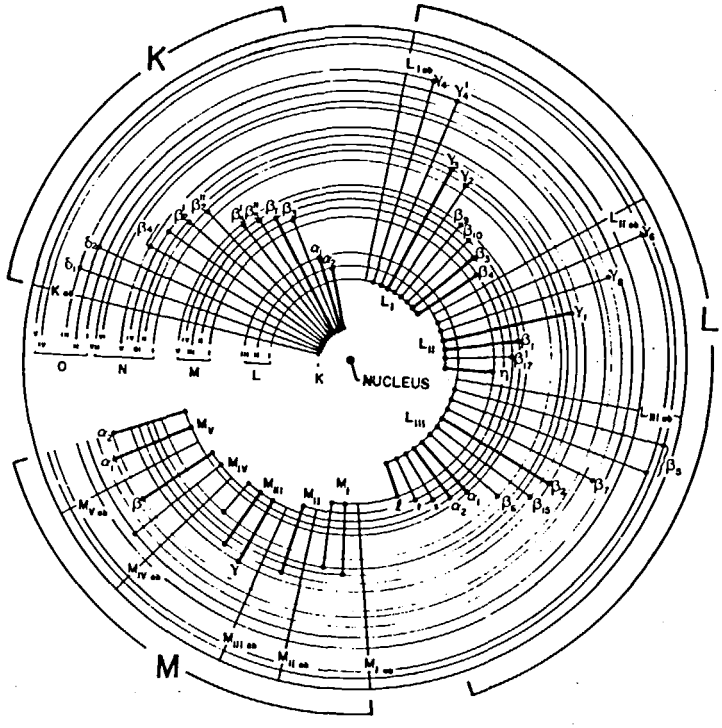

FIGURE 1. Atomic model, showing electron transitions and nomenclature. (From Woldseth, R., *X-Ray Energy Spectrometry*, Kevex Corp., Burlingame, 1973. With permission.)

A. Fluorescence

The vacancy may be filled by an electron transition from an outer shell, accompanied by the emission of a photon of energy $h\nu = E_f - E_i$, where E_f and E_i are the energies of the final and initial electron energy states. The energy of the photon is characteristic of the element and the shell or sub-shell of the atom between which the transitions take place. A complete transition scheme together with the recognized nomenclature is reproduced in Figure 1 (Woldseth[35]). The X-ray energy region most appropriate to PIXE is from 1 to 40 keV, which covers all the elements above sodium.

A map for the characteristic X-rays in this energy interval for elements $10 < Z < 92$ is reproduced from ASTM[36] and presented in Figure 2. A detailed tabulation of the X-ray energies of the different transitions and the absorption edges appropriate to each electron shell has been compiled by Storm and Israel.[37]

B. Auger Electrons

An alternative to the emission of an X-ray photon is the ejection of an outer electron from the atom. The initial inner-shell vacancy is removed by an electron transition from an outer shell, as in the previous case, and the energy available as a result of this transition results in the emission of an outer electron, known as an Auger electron. This Auger electron emerges with an energy equal to the energy difference between the energy released due to the initial electron transition and the binding energy of the Auger electron.

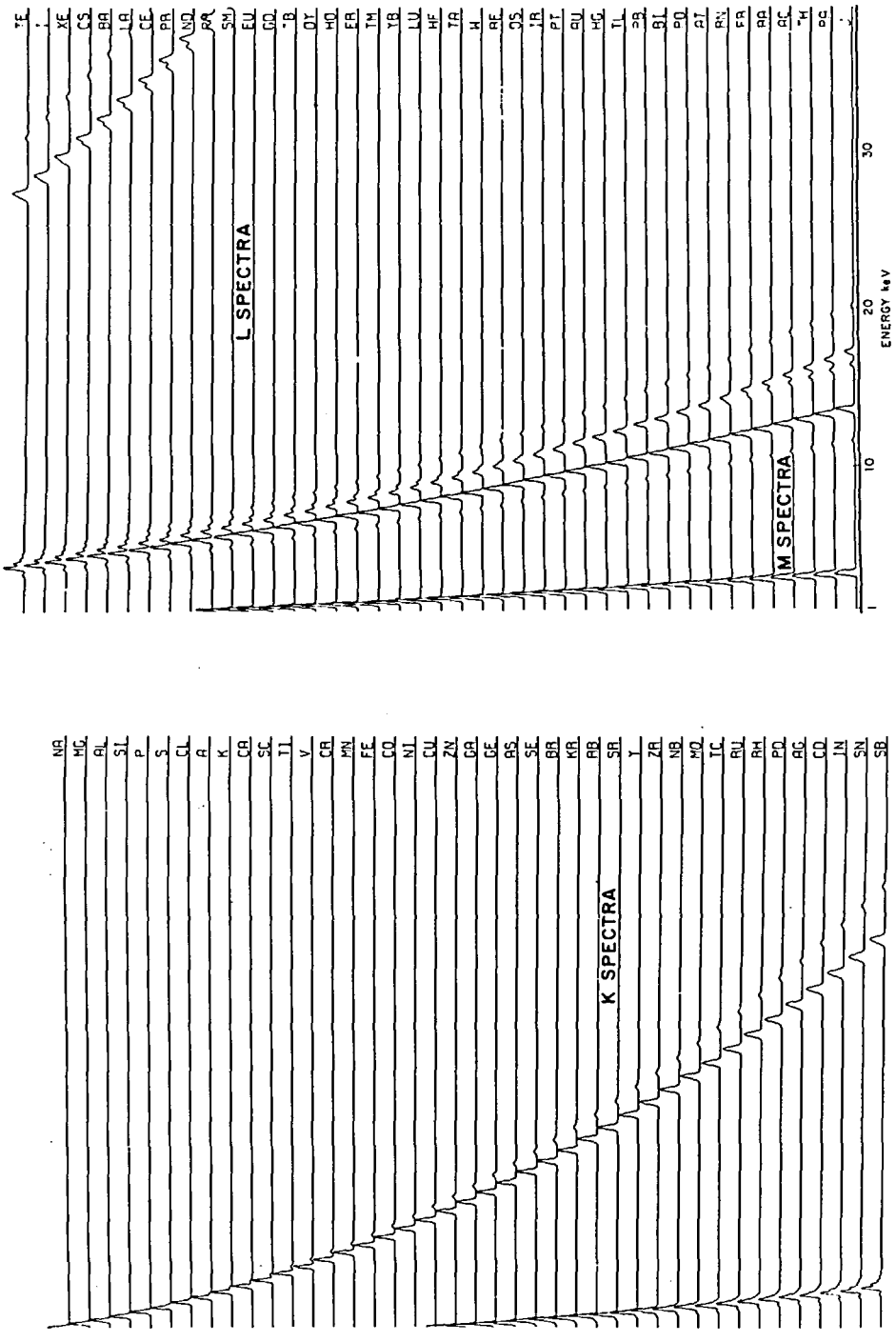

Calculated assuming 150 eV (FWHM) electronic noise and ε = 3.8 eV/e-h, F = 0.13.

FIGURE 2. Characteristic X-ray spectra from different elements, (From Russ, J. C., ASTM Special Technical Publication, 1971, 485. With permission.)

C. Coster-Kronig Transitions

With the exception of the K shell, all the electron shells are subdivided (Figure 1). If a vacancy is created in one of these subshells then radiationless transitions between subshells of the same shell can take place by virtue of their different angular momenta. By this process a vacancy may be moved to a higher subshell before being removed by an intershell transition. The net effect of these subshell transitions is a change in the primary vacancy distribution of the subshells. The transitions are known as Coster-Kronig transitions.

D. Fluorescence Yield

The ratio of the number of primary vacancies filled, giving rise to X-ray emission to the number of initial vacancies created, is termed the fluorescence yield of the atom. Conveniently, the fluorescence yield, ω, can also be expressed as the ratio of the X-ray production cross-section to the ionization cross-section and is given by $\omega = \sigma_x/\sigma_I$, where σ_x and σ_I are the X-ray production and the ionization cross sections, respectively. This definition as it stands is applicable to the K-shell only. For the other shells, which exhibit subshells, the primary vacancy distribution may change due to Coster-Kronig transitions and the situation becomes more complex. A detailed discussion of these phenomena and the appropriate expressions can be obtained from Bambynek et al.,[38] which also summarizes fluorescence yield data up to July 1971. These data have subsequently been augmented with recent data by Krause[39] to obtain an internally consistent set of best values for the fluorescence, Auger, and Coster-Kronig yields. For low Z elements, the emission of Auger electrons predominates. At higher atomic numbers the probability of the vacancies being filled and accompanied by the emission of X-rays increases, which is reflected in the variation of fluorescence yield with atomic number, Figure 3.

E. Cross Sections

Many aspects of multielemental analysis by PIXE require an accurate knowledge of the appropriate cross sections, which can either be obtained from experimental data or from theoretical studies. An early compilation of experimental measurements of K-shell ionization cross sections by Rutledge and Watson[40] revealed a general lack of consistent data in the proton energy region of 1 to 3 MeV and prompted a succession of experimental measurements. The results of these measurements have been collected in a compilation by Gardner and Gray[41] which covers K-shell ionization data from 1973 through 1977. For data after this date reference must be made to the literature. The situation with regard to L-shell data is not so satisfactory, since the last compilation, by Hardt and Watson,[42] was published in 1976.

A number of different theoretical models have been developed to describe the inner-shell ionization by charged particles from which the cross sections and their variation with energy can be extracted. These are the plane wave Born approximation (PWBA), binary encounter approximation (BEA), and the semi-classical approximation (SCA). It has been shown, however, by Madison and Merzbacher[43] and Taulbjerg,[44] that the BEA can be obtained from the PWBA theory by suitable choice of the representation of the emitted electron. In addition, Taulbjerg[45] has shown that the total cross sections obtained from SCA and PWBA are equivalent. Details of these models and extended tables from which the cross sections can be obtained have been published by Choi et al.,[46] Basbas et al.,[47] and Rice et al.,[48] (PWBA); Garcia et al.,[49] and Hansen,[50] (BEA), and Hansteen and Mosebekk,[51] and Hansteen et al.,[52] (SCA). The inner-shell ionization cross sections, when scaled by suitable factors and plotted against a suitable energy parameter, produce a universal curve for all projectile-target combinations. Figure 4, reproduced from Khan et al.,[53] shows the universal function predicted by the PWBA together with experimental

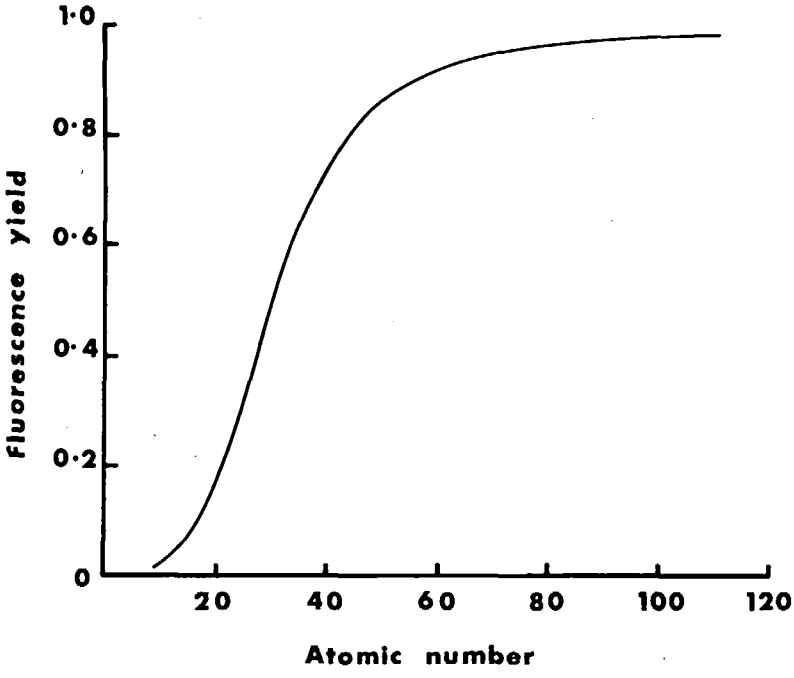

FIGURE 3. The variation of K-shell fluorescence yield with atomic number.

data on cross sections, reduced to the universal format in the manner described by Basbas et al.[47] The reduced cross sections, $\sigma_K/(\sigma_{oK}/\theta_K)$, are plotted against the universal variable $\eta_K/\theta_K^2.\sigma_K$ is the experimentally derived cross section, and σ_{oK} is the cross section scaling unit, given by

$$\sigma_{oK} = \left[\frac{Z_1}{Z_{2K}}\right]^2 8\pi \left[\frac{a_o}{Z_{2K}}\right]^2, \qquad (2)$$

which incorporates the target features. Z_1 is the atomic number of the incident particle, Z_{2K} the screened nuclear charge of the target and a_o the Bohr radius. The reduced projectile velocity parameter, η_K, proportional to projectile energy, is equal to the ratio of the squares of the incident particle velocity and the mean K-shell electron velocity of the target. The dimensionless parameter θ_K is given by (K-shell binding energy in eV)/13.6 Z_{2K}^2 and is an indication of the departure of the K-shell ionization energy from the hydrogenic form.

Benka and Kropf[54] have recently published tabulated data for K-shell and individual L-subshell cross sections using the universal format of PWBA. The authors have restricted themselves to protons as projectiles which has enabled exact analytical expressions to be employed for the maximum and minimum momentum transfer of the proton, instead of the more usual approximations. Corrections for increased binding energy and Coulomb deflection are incorporated at the appropriate energies. The cross sections obtained from these tabulations are in agreement with those of other tabulations for values of $\eta_K > 0.1$, to within 0.5% for the K-shell and 1% for the L-subshells. At low energies, $\eta_K < 0.1$, the predicted cross sections are smaller than those obtained using approximate methods to obtain the maximum and minimum momentum transfer.

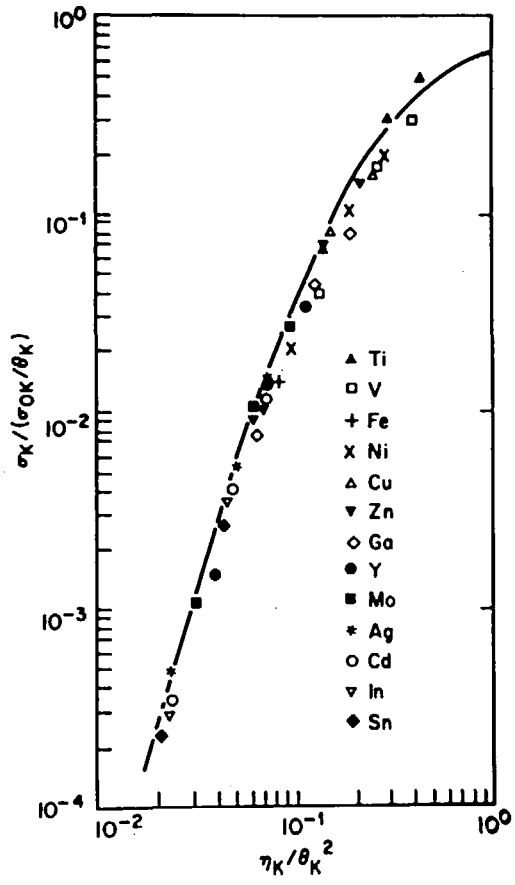

FIGURE 4. Comparison of reduced K-shell ionization cross section data with the universal function, solid line, predicted by the PWBA theory. (From Khan, M. R., Hopkins, A. G., Crumpton, D., and Francois, P. E., *X-Ray Spectrom.*, 6, 140 (1977). With permission.)

Brandt and Lapicki[55] have pointed out that large discrepancies exist between experimental L-cross sections and the plane wave Born approximation which can be accounted for by the CPSSR formulation of the plane wave Born approximation provided the projectile-target atomic number ratio $(Z_1/Z_2) \leqslant 0.3$. This approach incorporates the Coulomb deflection of the incident particle by the target atoms, the increase in electron binding energy for small impact parameters, the polarization of the electron shell for large impact parameters, and the relativistic effects on the target electrons. A detailed comparison of both of these latter approaches with the more recent experimental data has yet to be made.

From a practical viewpoint it is useful to know the qualitative behavior of the cross sections in terms of the energy and atomic number dependence. For values of $T_m \ll I_K$, the binding energy of the K electrons, Merzbacher and Lewis[56] have shown that the K-shell ionization cross section is proportional to T_m^4 and inversely proportional to I_K^6. Since I_K is proportional to Z_K^2, the effective atomic number for the K-shell electron, the ionization cross section is proportional to Z_K^{-12}, and to the fourth power of the proton energy, E_p^4.

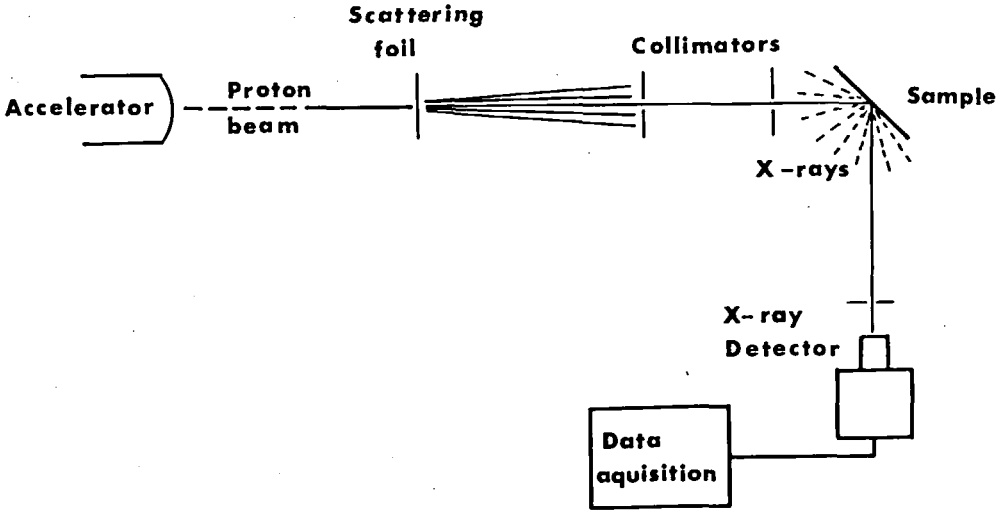

FIGURE 5. Schematic of typical PIXE system.

III. INSTRUMENTATION FOR PIXE ANALYSIS

The development of PIXE analysis has now reached the stage where the basic systems employed at the various centers employing the technique are all very similar in design concept. The essential features of such a system are shown schematically in Figure 5, and comprise (a) a beam of energetic charged particles, (b) a suitable target facility, and (c) a high resolution X-ray detector, together with a suitable data processing system. A beam of energetic protons, obtained from an appropriate accelerator, passes through a beam diffuser and a number of collimators before impinging on the sample under investigation. Normally, because of the short range of the protons in air, the sample is positioned in an evacuated target chamber. The X-rays generated by the passage of the protons through the target are detected by a lithium-drifted silicon, Si(Li), X-ray detector, which enables both the energy and the quantity of the emitted X-rays to be measured. The measurement of the X-ray energy facilitates the identification of the elements present in the sample while the X-ray yield (number of X-rays) permits a quantitative evaluation of the elements present.

A. Accelerators

Detailed studies have shown that the optimum sensitivity for PIXE analysis is obtained for protons with energies between 1 and 3 MeV, depending upon the element detected and the matrix material. As a consequence of this, the accelerators most widely employed for this purpose are mainly the variable energy Van deGraaff or Cockcroft-Walton machines capable of providing beams of protons with energies from 1 to 10 MeV and beam currents of a few microamperes. Access to such machines is no longer the problem it used to be since the transfer of many of the major nuclear physics research programs to machines of higher energy. Ideally the proton beam should be parallel, of uniform intensity, and, in many applications, of known area. This is achieved either by passing the beam through a thin diffuser foil and then collimating the resultant beam, as shown in Figure 5, or by sweeping the beam over the sample using electromagnetic deflectors.

The latter approach has been successfully employed by a number of workers, including Johansson et al.,[2] although it does require significantly more sophisticated apparatus than the former method. Akselsson and Johansson[34] obtained a homogeneous beam of 2.5 MeV protons by passing the beam through a 1.7 mg/cm^2 aluminum diffuser foil placed 60 cm in front of the target. A 7 mm diameter collimator was then employed to select a small region of the scattered beam. The homogeniety of the beam was checked using a beam mapping technique which employs a tiny moveable piece of metal to sample the beam as described in an earlier paper by Akselsson and Johansson.[57] Rickey et al.[58] also report the use of an aluminum foil to obtain an approximately uniform beam. The foil employed was 2.5×10^{-3} mm thick located 3 m from the target, and from the subsequent scattered beam a 16 mm diameter collimated beam was allowed to reach the target which is reported to be uniform to within 10%. The energy of proton beam employed is not, however, given. Montenegro et al.[59] have described in detail the procedure to follow to obtain a uniform particle beam for PIXE analysis. They employed a gold foil 110 μg/cm^2 thick to diffuse a 3 MeV proton beam, located 120 cm in front of the target. Their results for the measured profile of the beam with a diffuser foil present is shown in Figure 6 for a 2 mm diameter beam on target, which is somewhat smaller than that normally employed. Bauman et al.[60] discuss the physical characteristics of typical foil materials, nickel, gold, and tungsten, and conclude that high Z materials are the most appropriate as they have minimum energy loss per collision. The integrity of the foil is thus maintained over longer periods of time. Tungsten foils (2.5 μm) with a melting point of 3410° C, were found to last 3 to 4 days with beam currents up to 3 μA and energies of 3 MeV. The energy loss in a 2.5-μm tungsten foil is, however, quite considerable, of the order of 500 keV. It should be borne in mind that the diffusing systems described select only a small percentage of the diffused beam, the rest is deposited on the collimators. Hence the diffusing foil has to carry substantially more current than the target, which under appropriate conditions could be more than an order of magnitude greater. Regular inspection of the diffuser foil is therefore required to check its integrity.

B. Target Chamber

In the majority of cases the samples to be analyzed have been positioned within the vacuum system in a specially designed target chamber having suitable target mounting facilities. The characteristic X-rays produced can be detected external to the chamber, by arranging for them to pass through a thin exit window of melinex of thickness 50 μm. If it is intended to detect the low energy X-rays from the lighter elements then a suitable detector can be mounted within the vacuum system. The configuration of a typical target chamber is shown in Figure 7. For thin targets, through which the beam passes without significant loss of energy, the beam current is measured from the charge deposited in a suitable Faraday cup. A solid-state surface barrier detector is often incorporated at some backward angle to the incident proton beam so that observations can be made of the Rutherford backscattered protons from which the thickness of the sample can be deduced. It also enables Rutherford backscatter analysis (RBS) to be done simultaneously. If an external beam facility is required this can also be achieved by the provision of a suitable rear window.

For work involving samples thicker than the range of protons in the sample the beam current has to be measured on the sample. To enable this to be done accurately suitable electron suppressors must be provided so that electrons emitted from the sample under proton bombardment are not lost from the measuring system, or alternatively the entire chamber can be isolated and acts as a Faraday cup. In the case of nonconducting samples, a thin conducting film has to be evaporated onto the surface to render it conductive as described by Papper et al.[61] A liquid nitrogen cold trap must be employed whenever there

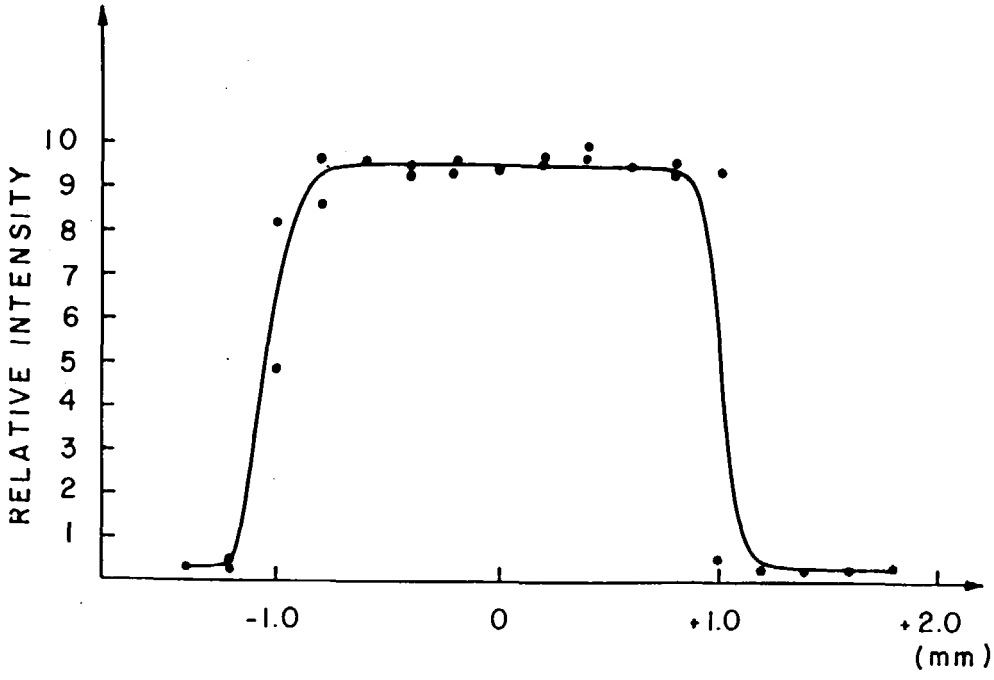

FIGURE 6. Profile of 3 MeV proton beam after diffusing with a 110 $\mu g/cm^2$ thick Au diffuser, (From Montenegro, E. C., Baptista, G. B., Leite, C. V. B., De Pinho, A. G., and Paschoa, A. S., *Nucl. Instrum. Methods,* 164, 231 (1979). With permission.)

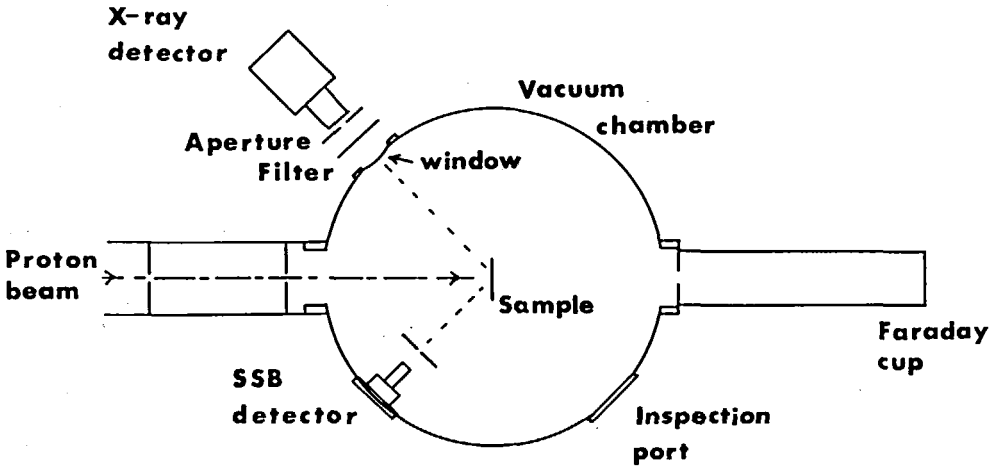

FIGURE 7. Typical target chamber configuration employed in PIXE analysis.

is a possibility of loss of material from the sample during proton bombardment, as is sometimes the case with biological samples. Material lost from the sample condenses on the cold trap and prevents contamination of the system.

Due to the time involved in mounting a sample for analysis in the chamber, evacuating the chamber, and then obtaining the desired beam on the sample, multiple sample facilities are essential. Facilities such as this have been described by several authors

including Feld and Umbarger,[62] Mangelson et al.,[10] and Valkovic et al.[63] Barnes et al.[16] used the principle employed in an ordinary slide projector to change the samples in their multiple sample assembly, a technique also employed by Orsini and Boueres[64] and Akselsson and Johansson.[34] Typically the samples are mounted in conventional 5×5 cm slide mounts, 40 of which can be carried in a typical slide changer. Lecomte et al.[65] report the use of a carousel-type slide changer carrying up to 80 sample slides. Samples have also been installed on sample ladders carrying a number of samples which can be stepped sequentially into the proton beam as described by Jolly et al.[66] The choice of facility obviously depends on the nature of the samples to be analyzed, and most laboratories have alternative mounting facilities available.

Problems relating to background radiation reaching the detector from collimators and the sample chamber can be reduced by suitable choice of materials and by lining the chamber with carbon foil as described by Raith et al.[67]

To minimize the heating due to the beam and reduce loss of volatile elements, Jolly et al.[66] rotated the sample spreading the beam over a 2 cm diameter annulus. In addition, the chamber was filled with helium at a pressure of 100 torr, rather than evacuated as is normal practice. This system, used with very thin carbon-impregnated polycarbonate backings, enables a few microamperes of beam to be employed without any significant loss of volatile elements. Similarly, Bauman et al.[60] operate their sample chamber helium filled, but at atmospheric pressure, and have observed no damage at beam currents of 200 nA and 2 MeV. In addition, charge build up on insulating samples is prevented. The kapton foil between the vacuum and the helium reduces the proton energy by about 400 keV, and this is further reduced 125 keV by the helium. It should be stressed, however, that Si(Li) detectors must not be operated in a helium atmosphere as the helium diffuses through the beryllium window causing loss of vacuum in the detector housing leading to detector failure.

C. X-Ray Detection System

High resolution lithium-drifted silicon detectors, Si(Li), for the detection of characteristic X-rays, are now well established in such fields as electron probe microanalysis, radioisotope X-ray fluorescence, and ion-induced X-ray emission analysis. Their widespread use has almost obscured the use of proportional counters, NaI(Tℓ) detectors, and crystal spectrometers in the analysis field. Although the resolution of the Si(Li) detector is not as good as that of an X-ray crystal spectrometer, resolutions are such that characteristic X-rays from neighboring elements can be readily distinguished. In addition, a Si(Li) detector system can analyze X-rays of different energies simultaneously and has a detection efficiency of nearly 100% for X-rays of energies 4 to 30 keV, depending on the detector thickness.

Si(Li) detectors are cooled to liquid nitrogen temperatures to reduce thermal noise and prevent diffusion of the lithium through the crystal. The lithium creates an intrinsic region within the silicon which can be regarded as a solid-state ionization chamber. X-rays absorbed in this region lose their energy by excitation and ionization of the absorbing atoms thus producing electron-hole pairs. On average, the energy required to produce an electron-hole pair is 3.62 eV in silicon at room temperature and is independent of the incident X-ray energy. The electron-hole pairs created are collected by the application of a suitable high voltage (typically 750 to 1500 V) applied across the intrinsic region. If a photon of energy E is absorbed in such a detector the number of electron-hole pairs produced, n, is given by

$$n = \frac{E(\text{in eV})}{3.62}, \qquad (3)$$

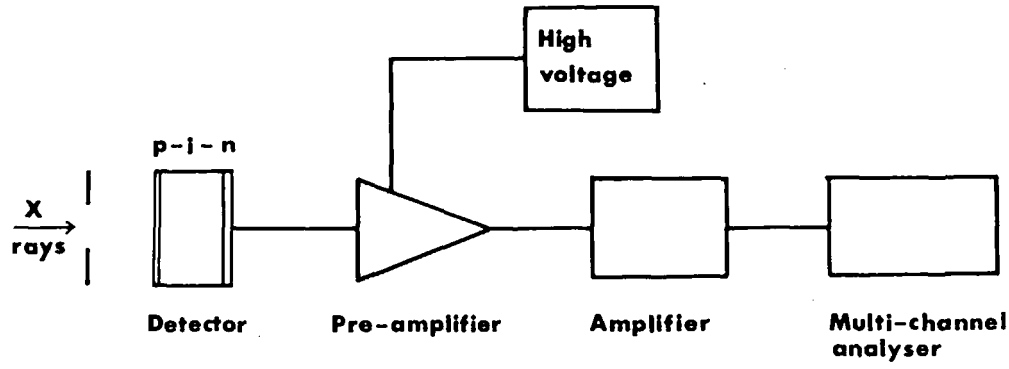

FIGURE 8. Schematic of a Si(Li) X-ray detection system; p-i-n refers to p-type, intrinsic, and n-type silicon, respectively.

from which the total charge deposited in the crystal can be deduced. Hence, the charge collected is linearly proportional to the energy of the X-ray absorbed in the detector. It should be noted that the entrance window to the detector is extremely thin beryllium. This window must not be touched as this will result in serious damage to the detector.

A typical Si(Li) X-ray detection system is shown schematically in Figure 8. The small quantity of charge collected by the application of the high voltage to the detector is amplified by the charge-sensitive preamplifier before being transmitted to the main amplifier for further amplification and pulse shaping. The pulse heights of the output pulses from the main amplifier are proportional to the energy of the X-rays producing these pulses. It is necessary, therefore, to distinguish between pulses of different pulse heights, and this is accomplished using a multichannel pulse height analyzer.

1. Resolution

The energy resolution of the X-ray detection system is a measure of its ability to distinguish between two X-rays of similar energy. The resolution of the modern Si(Li) detector is such that the noise and count rate capability of the associated electronics can be the limiting factors governing the overall resolution. A typical X-ray spectrum obtained with a Si(Li) detector system is shown in Figure 9, giving the response of the system to the K_α and K_β X-rays of manganese. The resolution of the system is conveniently expressed as the full width of the energy peak at one half of its maximum intensity (FWHM) measured in energy units. For the example given, the resolution of the manganese K_α peak is 160 eV. Since the resolution varies with energy, it is necessary to quote the energy at which the measurement is made, in this case 5.895 keV. It has been generally agreed that to facilitate the intercomparison of different detector systems that the resolution should be quoted for the Mn K_α X-ray, since this can be readily obtained from a radioactive ^{55}Fe source.

The broadening of a recorded X-ray peak is due to two effects. The first is the uncertainty in the number of charges produced by an X-ray, and is an intrinsic property of the detector associated with the ionization statistics. This contribution to the broadening, $\Delta E_{(detector)}$ is given by

$$\Delta E_{(detector)} = 2.35\,(E\bar{\epsilon}F)^{1/2}\ eV. \qquad (4)$$

where E = energy of detected radiation in eV, $\bar{\epsilon}$ = average energy to produce an electron-hole pair, F = Fano factor and is a property of the material = 0.13 for silicon.

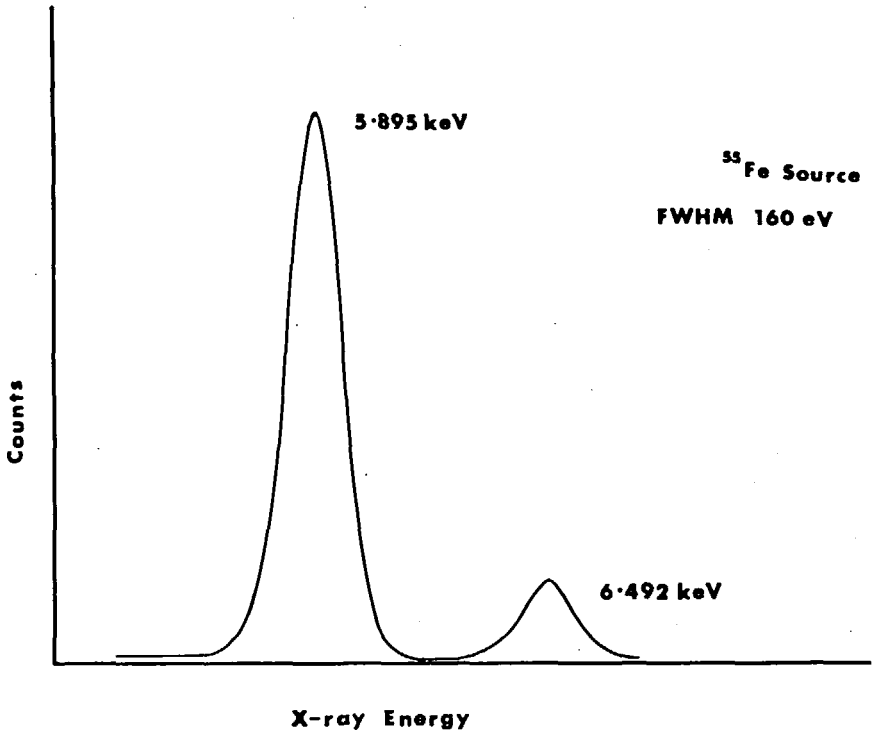

FIGURE 9. Manganese X-ray spectrum obtained from a ^{55}Fe source recorded with a Si(Li) detector, resolution, FWHM, 160 eV.

The constant 2.35 relates one standard deviation of a Gaussian distribution to the FWHM. The second source of broadening is noise which results from the leakage current in the detector and noise in the associated electronics. The total full width half maximum of the observed peak, FWHM, is expressed as the quadratic sum of these two components,

$$\text{FWHM} = \left[(\Delta E)^2_{\text{NOISE}} + (2.35\,(E\bar{\epsilon}F)^{1/2})^2 \right]^{1/2} \qquad (5)$$

A significant contribution to the noise arises from the preamplifier and to keep this contribution to a minimum the first stage of the preamplifier in the form of a FET is cooled to liquid nitrogen temperature, as is the detector to inhibit diffusion of the lithium. The noise component is independent of the incident X-ray energy and can be most conveniently measured using a precision pulser applied to the preamplifier input.

For multielemental analysis, particularly for the elements of low atomic number, resolution is very important because of the small differences in energy of the characteristic radiations. There are about 20 elements with K X-ray energies between 1 and 10 keV which makes their identification extremely difficult. The L X-rays from the elements with $35 < Z < 50$ also fall in this already crowded region below 10 keV, thus making the situation more complex. Fortunately, neighboring elements in the low Z region do not always occur together in an analysis.

2. Detector Efficiency

The efficiency of a Si(Li) detector to X-rays depends on the energy of the X-ray, detector thickness, and the entrance window employed. The approximate detection

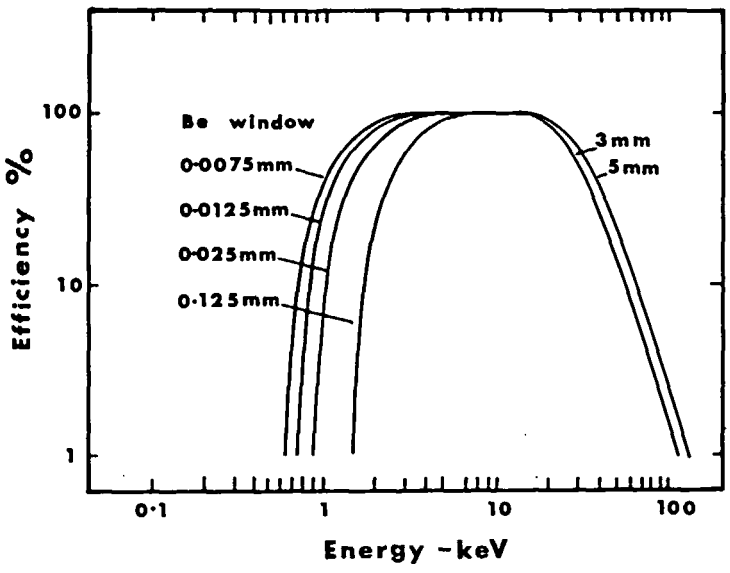

FIGURE 10. The variation of efficiency of a Si(Li) detector with X-ray energy for 5 mm and 3 mm thick detector crystals with different thicknesses of entrance window.

efficiency can be calculated, assuming a narrow beam geometry, from the expression $\epsilon = (1\text{-}e^{-\mu_2 x_2})\, e^{-\mu_1 x_1}$ where x_1 and x_2 are the thicknesses of the window and detector, respectively, and μ_1 and μ_2 are the appropriate energy dependent absorption coefficients. The results of such a calculation are shown in Figure 10 for 5 mm and 3 mm thick detector crystals with different thicknesses of entrance windows. These curves have two distinct features, a fall in efficiency at high energies and low energies. At energies above 15 keV, the fall in detector efficiency is due to the increased transmission of the X-rays through the detector crystal which is clearly more pronounced on the thinner crystal. Below 7 keV, the detector efficiency falls sharply due to the absorption of the incident X-rays in the beryllium window and any silicon dead layer.

Since detector specifications, as supplied by manufacturers, are only nominal, coupled with the fact that the thickness of any dead layer on the surface of the detector crystal is unknown, it is useful to measure the efficiency experimentally. If the detector is to be employed in the region below 4 keV, where the efficiency changes rapidly with energy, it is essential that the efficiency be experimentally determined. In a very comprehensive investigation into the response of semiconductor detectors Hansen et al.[68] point out that a 500-nm dead layer on a silicon crystal absorbs 10% of incident photons of energy 3 keV. They observed that the detection efficiency can change due to temporal variations in the detector parameters and also due to thermal cycling, and hence recommend that the efficiency should be checked experimentally from time to time.

Several different experimental approaches have been employed to obtain the efficiency of Si(Li) detectors. Hansen et al.[68] employed the absolute photon emission rates of X-rays and gamma rays from carefully calibrated radioactive sources and determined the efficiency with a precision of 5% above 6 keV and 5 to 10% from 3 to 6 keV, the precision at the lower energies being limited mainly by the self-absorption of the low energy radiations in the calibrated sources. Wood et al.,[69] in a detailed study of detector efficiencies, employed this technique to calibrate the efficiency of a Si(Li) detector from 5 to 170 keV with a precision on individual measurements of about 4%. The sources employed, listed in Table 1, were either calibrated IAEA sources or sources calibrated in

Table 1
CALIBRATION SOURCES

Source	Energy (keV)	Half life	Calibration method
^{54}Mn(Cr K)	5.4	312.6 d	NaI(Tl)cc
^{55}Fe(Mn K)	5.9	2.60 y	NaI(Tl)cc
^{57}Co(Fe K)	6.4	271.6 d	NaI(Tl)cc
^{65}Zn(Cu K)	8.0	245 d	NaI(Tl)cc
^{75}Se(As K)	10.5	120.4 d	NaI(Tl)cc
^{241}Am(Np Lι)	11.9	432.9 y	IAEA
^{241}Am(Np Lα)	13.9	432.9 y	IAEA
^{57}Co	14.4	271.6 d	NaI(Tl)cc
^{88}Y(Sr K)	14.1	107.4 d	NaI(Tl)cc
^{241}Am(Np Lβ)	17.8	432.9 y	IAEA
^{241}Am(Np Lγ)	20.8	432.9 y	IAEA
^{109}Cd(Ag Kα)	22.1	453 d	NaI(Tl)cc
^{113}Sn(In Kα)	24.2	115 d	NaI(Tl)cc
^{109}Cd(Ag Kβ)	24.9	453 d	NaI(Tl)cc
^{241}Am	26.3	432.9 y	IAEA
^{113}Sn(In Kβ)	27.3	115 d	NaI(Tl)cc
^{210}Pb	46.5	21 y	NaI(Tl)13
^{241}Am	59.5	432.9 y	IAEA
^{57}Co	122.0	271.6 d	IAEA
^{57}Co	136.3	271.6 d	IAEA
^{139}Ce	166	140 d	NAI(Tl)13

From Wood, R. E., Roe, P. V., Puckett, O. H., and Palms, J. H., *Nucl. Instrum. Methods*, 94, 245 (1971). With permission.)

situ using a NaI(Tℓ) detector system. Gehrke and Lokken[70] also employed a NaI(Tℓ) detector system to determine the absolute emission from suitable sources, which were prepared by depositing small quantities of radioactive solutions of high specific activity onto plastic films. The sources were then employed to calibrate a Si(Li) detector from 5 to 125 keV with a precision of approximately 7%. Gallagher and Cipolla[71] report the calibration of a Si(Li) detector down to 3.3 keV using the same technique and suggest that the use of L and M X-rays could be usefully employed to extend the measurements down in energy towards the silicon K absorption edge at 1.84 keV. The practice of employing NaI(Tℓ) detectors for the absolute determination of low energy photons is not without its difficulties, such as the correct treatment of escape peaks and backscatter contributions, as has been pointed out in a detailed study by Campbell and McNelles[72] and Campbell et al.[73] To overcome these problems Campbell utilized radioactive sources which emitted simultaneously gamma rays of moderate energy and K X-rays, the relative intensities of which are accurately known. The K X-rays arise either as a result of electron capture or internal conversion. The absolute gamma ray emission rate was obtained using a calibrated Ge(Li) detector and the known ratios used to determine the Si(Li) detector efficiency. A critical review of the decay data of appropriate sources for calibration in the energy range of 5 to 40 keV is presented by Campbell.

Both of these approaches, however, suffer from the limitations imposed by using low energy radioactive sources, such as self-absorption, uncertainties in the decay schemes, and the general lack of suitable sources in the critical energy region below 7 keV. In an alternative approach, Johnson et al.[74] obtained the efficiency of a Si(Li) detector by using the fluorescent radiation from a series of targets exposed to the 59.5 keV photons from a 100 mCi ^{241}Am source. An overall uncertainty of $\pm 3\%$ was estimated for the energy range

Table 2
TARGET MATERIALS AND RADIOACTIVE SOURCES EMPLOYED FOR THE DETERMINATION OF THE EFFICIENCY OF A Si(Li) DETECTOR

X-ray	Mean X-ray energy	Target material
Fe L	0.71	Plate
Co L	0.78	Plate
Ni L	0.86	Plate
Cu L	0.94	Plate
Zn L	1.02	Plate
Na K	1.04	NaCl, evaporated
Mg K	1.25	Plate
Al K	1.49	Plate
Si K	1.74	Evaporated
Zr L	2.07	Plate
Mo L	2.3	Plate
Cl K	2.7	NaCl, evaporated
Ca K	3.7	Evaporated
Ti K	4.6	Plate
Cr K	5.5	Plate
Cr K	5.5	^{54}Mn
Mn K	6.0	^{55}Fe
Fe K	6.5	^{57}Co

From Shima, K., *Nucl. Instrum. Methods*, 165, 21 (1979). (With permission.)

5 to 30 keV. This method is obviously very convenient and does not involve the preparation of a large number of radioactive sources, as the fluorescent targets used are stable isotopes. The absolute emission rate of the fluorescent radiation was obtained from a calibrated NaI(Tℓ) detector and so the technique does suffer from the limitations imposed by the use of such detectors. The results of this study indicated that the active region was thinner than specified resulting in an efficiency less than anticipated. In addition, a noticeable fall in efficiency was observed below 15 keV, attributed to absorption in a dead-layer and the gold bias contact.

The recent work of Shima[75] is noteworthy in that it extends the efficiency determinations down to 0.7 keV. This was achieved by comparing the yield of proton-induced characteristic X-rays from selected targets, as measured by the Si(Li) detector, with that obtained using a proportional counter of known efficiency. A series of 15 measurements were made in the critical energy region below 7 keV using this approach together with 3 measurements on radioactive sources. The targets and sources employed, together with their energies, are listed in Table 2. Their results, which are shown in Figure 11, have an experimental uncertainty of less than 8% for X-ray energies greater than 1 keV and clearly show the discrepancies between calculated and experimental efficiencies.

3. Detector Electronics

The semiconductor input stage to the spectrometer system, shown schematically in Figure 8, is most conveniently represented electronically by its equivalent circuit shown in Figure 12. C is the total capacitative load presented to the preamplifier and comprises the capacitance of the depletion layer of the detector together with stray capacitance of

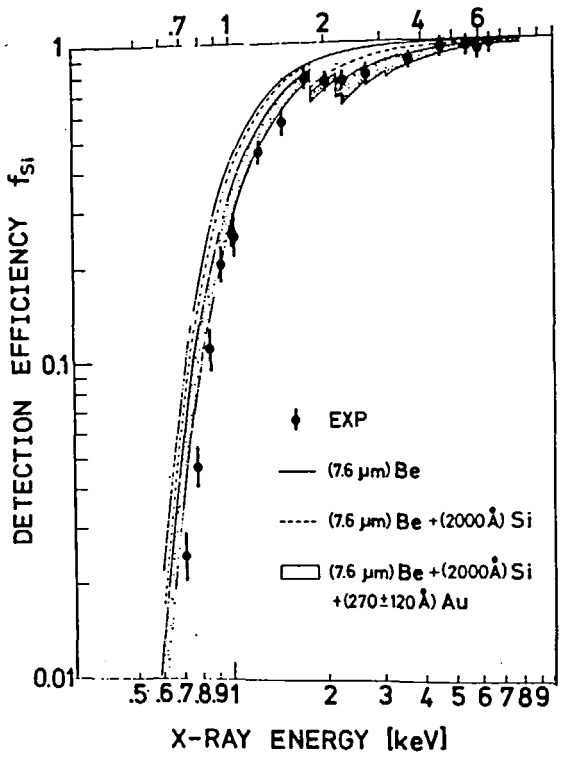

FIGURE 11. Experimentally determined Si(Li) detector efficiencies in the low energy region compared with calculated efficiencies with surface layers of Be, Be + Si, and Be + Si + Au. (From Shima, K., *Nucl. Instrum. Methods,* 165, 21 (1979). With permission.)

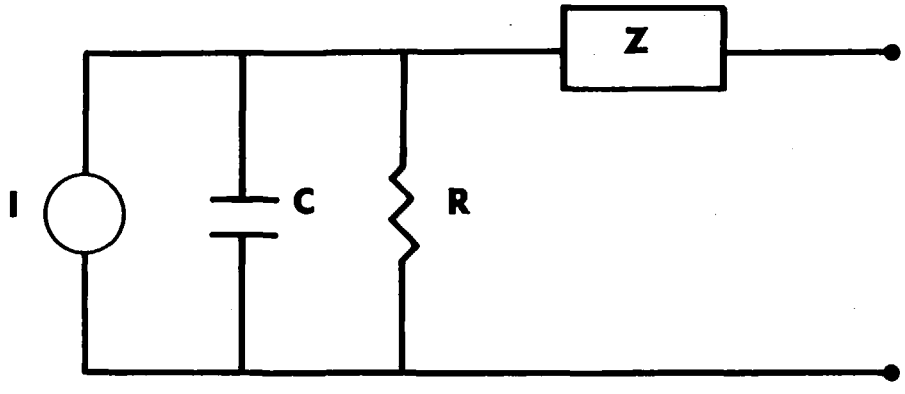

FIGURE 12. The equivalent circuit representation of a Si(Li) detector.

cables and connectors. R is the resistance of the depletion layer and Z the series impedance due to any dead-layer or constant resistance. The charge created in the detector by the interacting X-ray is collected by the applied bias voltage and thus a current flows through the detector, represented in the equivalent circuit by the current generator. The random addition of noise charges, charges lost due to incomplete charge

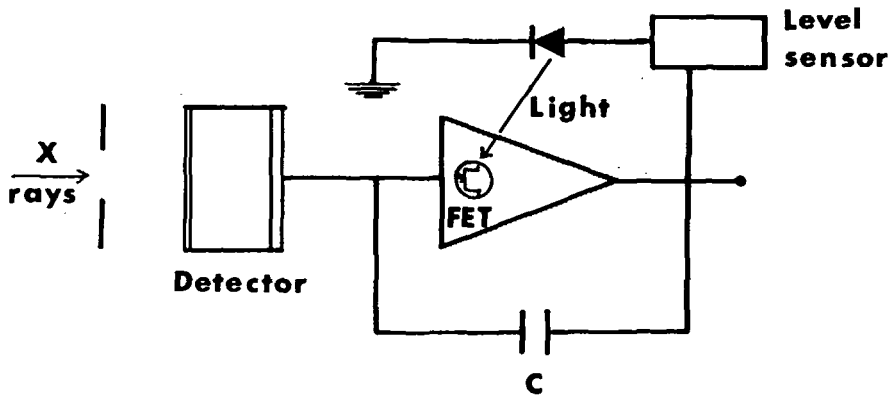

FIGURE 13. Schematic of a pulsed optical feedback preamplifier system.

collection, and statistical fluctuations, contribute to the nonlinearity of the output pulse and loss of resolution.

The charge-sensitive preamplifier integrates the charges produced in the detector and presents them as a voltage signal to the main amplifier. To obtain optimum noise suppression, and hence better resolution, the first stage of the preamplifier is a field effect transistor (FET) matched to the detector for optimum signal-to-noise ratio and cooled with the detector to liquid nitrogen temperature. To keep the operating condition of the FET unaltered, a feedback path from the preamplifier output to its input must be provided. In the resistor feedback preamplifier, a resistor is connected in parallel with the FET, but this resistor acts as source of noise and lengthens the pulses affecting the count rate capability adversely. An alternative offered by manufacturers is a pulsed optical feedback system, shown in Figure 13. In this system the output of the FET is allowed to build up in steps to a preset level, at which point a level sensor triggers a light-emitting diode. This light shines momentarily on the FET drain gate junction, making it conductive, thus allowing the capacitance to discharge and reset the system. A pulsed optical system such as described has good performance in terms of resolution and low noise characteristics but has limited count rate capability.[35] Preamplifiers employed have a typical input charge conversion of the order of 4.5 mV output per 10 keV of energy deposited in the crystal. The output impedance is typically 50 or 75 ohms.

The somewhat small output signal from the preamplifier is further amplified and shaped by the main amplifier to render it compatible with the subsequent processing equipment. Modern amplifiers are equipped with a bias level, post gain, course gain and fine gain, together with facilities for varying the time constants of the system. Long shaping time constants are necessary for efficient noise suppression and to define the pulse height accurately prior to its measurement. An increase in pulse shaping time does, however, lead to a greater probability of pulse pile up and as a consequence a decrease in the count rate performance.

4. Sum Peaks and Pulse Pile Up

The use of long shaping time constants in the main amplifier, for optimum energy resolution, enhances the probability that while one pulse is being processed another pulse arrives, resulting in an overlap of the two pulses in the main amplifier. Three types of pile up are possible as illustrated in Figure 14 (Woldseth[35]).

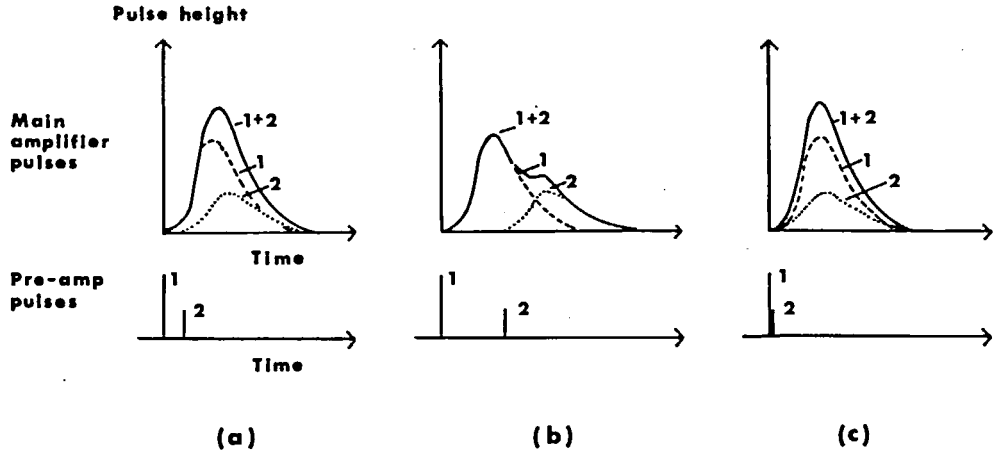

FIGURE 14. Pulse pile up effects in the main amplifier, due to the long pulse shaping time-constants employed (From Woldseth, R., *X-Ray Spectrometry*, Kevex Corp., Burlingame, 1973. With permission.)

Leading edge — This is the situation shown in (a). A second pulse arrives before the first pulse has reached its maximum value as determined by the shaping time constants in the amplifier. The result of this is that the two original pulses are lost and replaced by a single pulse whose height is a combination of the two initial pulses. A change in pulse height is extremely undesirable since the pulse height is used as a measure of the incoming X-ray energy.

Trailing edge — This is illustrated in (b). Here the second pulse arrives after the first pulse has crossed at peak amplitude and is in the second part of its processing time. The height of the first pulse remains unaltered, but the second pulse suffers a change in pulse height and shape, leading to degradation of system resolution.

Sum peak — The third possibility is shown in (c), where two pulses arrive at essentially the same time at the main amplifier. This results in the formation of a single pulse the height of which is the sum of the individual pulses. For monoenergetic X-rays this results in a peak in the spectrum at twice the energy of the incident radiation.

5. Pulse Pile Up Rejector

The distortion of pulses described above can be overcome by the use of a pulse pile up rejector which enables the linearity between the energy of the photon and the output pulse to be maintained. This is achieved by the rejection of pulses distorted by the pile up processes described earlier. In leading edge pile up the amplitude of both pulses is distorted and both have to be rejected. In trailing edge pile up only the second pulse is distorted and needs to be rejected. These operations are performed in a typical pulse pile up rejector in the following manner. The pulses from the preamplifier go first to a fast amplifier with good pulse pair resolution (i.e., the ability to measure the time between successive pulses) before being passed to the main amplifier for shaping. If the time separation between pulses, as measured at the fast discriminator, is less than the total width of the shaped pulse in the main amplifier, a gate prohibits passage of both pulses in the case of leading edge pile up, or of only the second pulse in the case of trailing edge pile up. The total width of the quasigaussian shaped pulses in the main amplifier is taken as $10\,\tau$, where τ is the time constant employed. The performance of a typical pulse pile up rejector system is shown in Figure 15 (Woldseth[35]). In the case of the sum pile up this can only be reduced by keeping the counting rate down to an acceptable level.

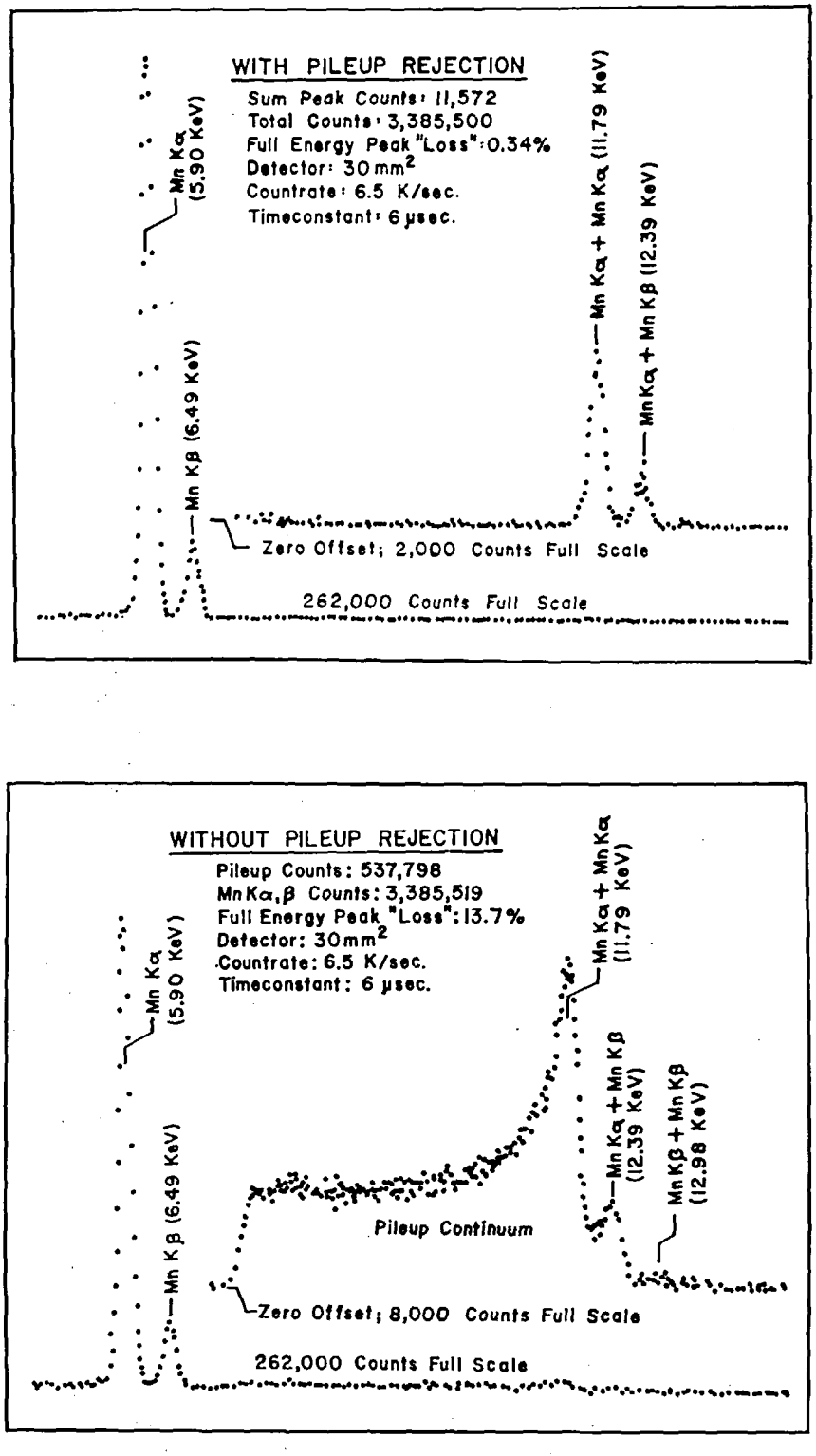

FIGURE 15. Performance of a typical pulse pile up rejector circuit. (From Woldseth, R., *X-Ray Spectrometry*, Kevex Corp., Burlingame, 1973. With permission.)

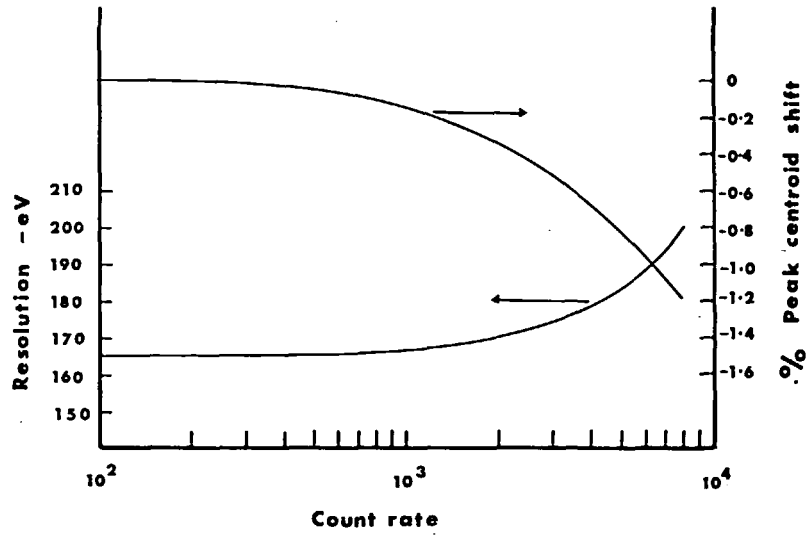

FIGURE 16. Resolution and peak centroid shift as a function of counting rate.

6. Resolution and Baseline Stability

At high counting rates problems can occur with the stability of the DC level of the amplifier resulting in a loss of resolution and a shift of the centroid of the X-ray peak. Commercially available DC restorers or baseline restorers may be used to counter this effect. The resolution as a function of input count rate is shown in Figure 16. For the time constants employed in this example the system resolution decreases very rapidly as the counting rate is increased beyond 2000 Hz. The magnitude of the peak centroid shift observed at high counting rate is also shown.

7. Multichannel Analyzer

Since the heights of the output pulses from the amplifier are proportional to the X-ray energy it is necessary to sort the pulses according to pulse height so that the number of pulses corresponding to a given energy is known. This is achieved using a multichannel analyzer, which consists essentially of an analog-to-digital converter (ADC) and a memory store. The purpose of the ADC is to convert the analog signal from the amplifier into a digital signal so that it can be stored in the memory. As described by Gedcke[76] a discharged capacitor is charged by the voltage output pulse of the amplifier until its voltage is equal to the maximum voltage of the applied pulse. The capacitor is then discharged linearly with the result that the discharge time is proportional to the initial pulse height. A train of pulses from an oscillator is generated during the discharge time which is employed to locate the position in the memory corresponding to the appropriate pulse height. The store at this position in the memory is then incremented by one. The entire process is then repeated for the next pulse, thus generating an energy spectrum in the memory store of the multichannel analyzer.

8. Dead Time Corrections

Whether a pulse pile up system is employed or not the long shaping time constants of the amplifier, which are necessary to achieve adequate resolution, result in the loss of pulses from the spectrum, as does the finite processing time of the ADC, both of which must be corrected for if accurate quantitative results are to be obtained. Modern pulse height analyzers are equipped with address clocks with frequencies in excess of 50 MHz

to reduce the processing time and hence the dead time of the ADC. A detailed discussion of the self-prolonging dead time appropriate to Si(Li) spectrometer systems can be found in the paper by Reed,[77] who has investigated dead time effects as a function of input counting rates. This study shows that X-ray peak intensity measurements can be made at total count rates of up to 10,000 Hz, with a precision of 1% if appropriate corrections are made. Many pulse pile up rejector circuits furnish a busy signal output, so that corrections can be made electronically. This signal often takes the form of a 5 V level maintained only while a pulse is processed. This signal can be employed to gate the multichannel analyzer clock timer, and calculation is then made on the basis of the so-called "live" time. Some computer-based multichannel analyzers do not have easy access to the appropriate clock timer and an alternative approach, such as described by Khan and Crumpton,[78] must be employed. They employed a 100 kHz crystal oscillator, the output of which was gated by the busy signal. This gated output, connected to a scaler after suitable division, gives the live time directly. It should be borne in mind, however, that proton beams have time structure. A more satisfactory approach, therefore, is to employ the busy signal to gate the beam charge measurements so that the effect of temporal variations is removed, and the X-ray yield can be normalized directly to the beam charge.

The electronic approach described, although adequate at relatively low counting rates, runs into difficulties of a practical nature as the counting rate is increased above 1 kHz. As pointed out by Rickey et al.,[58] with an active time constant of 4 μs and a counting rate of 10 kHz, 60% of the pulses are rejected leading to unacceptably long counting periods. An alternative approach, first proposed by Jaklevic et al.[79] and subsequently evaluated by Cahill,[80] is based on a system of on-demand beam pulsing. The procedure adopted is to sweep the proton beam electrostatically off the sample as speedily as possible following the arrival of an X-ray at the detector. Only when the measurement of the pulse is completed is the beam returned onto the sample. This approach has been used successfully by several authors, including Rickey et al.,[58] Koenig et al.,[81] Mingay et al.,[82] Akselsson and Johansson,[34] and Van der Heide et al.[33] The beam deflection is accomplished by passing the beam between two parallel electrostatic plates situated 2 to 3 m from the sample. The voltage on one of the plates is grounded each time an X-ray is detected, causing the proton beam to be deflected to a well-shielded beam stop. The beam is maintained on the beam dump for a time proportional to the processing time of the X-ray signal and then returned onto the sample, having made due allowance for the time of flight of the protons from the deflector plates to the sample. Counting rates of up to 10 kHz are reported without significant loss of any pulses. This clearly is highly advantageous as it results in a much shorter analysis time and requires no dead time correction. In addition, Mingay et al.[82] and Koenig et al.[81] report better system resolution at all counting rates and a maximum statistical precision obtained on the X-ray yield in a minimum time. In this later respect the system is self-regulating, since an increase in X-ray yield results in the beam being kept off the sample for a proportionally longer interval of time and vice versa, so that the system is always run at the optimum counting rate.[80] The system as described is not absolutely free of pulse pile up because of the time taken between detection of the X-ray and the removal of the beam from the sample, typically 200 or 300 ns. This very small contribution, however, can be easily handled with a conventional pulse pile up rejector circuit.

D. Computerized Data Analysis

In order to exploit the full multielemental capability of PIXE and enable large numbers of samples to be processed on a routine basis it is desirable to have a fully automated system employing computer evaluation of the complex multielemental

spectra. Ideally the computer program should be capable of locating and identifying all possible X-ray peaks, including multiplets, from elements ranging from phosphorus to uranium. It should accurately determine the concentration of the elements in the sample for a variety of experimental conditions in a minimum of time with little or no operator participation. It should be capable of dealing with interferences and should inform the operator when ambiguities arise. In aiming for this a number of different approaches have been investigated.

An obvious starting point for many laboratories was to employ existing programs designed to evaluate γ-ray spectra, suitably modified for the evaluation of X-ray spectra.[83-85] Johansson et al.[86] report the use of one of these, SAMPO (Routti and Prussin[84]), which fits a Gaussian function with exponential tails to the X-ray peaks and a polynomial representation of the background in the region of interest. This code, however, can only accommodate up to six peaks at any one time, is rather slow, requires a large computer, and significant operator participation. Lin et al.,[23] in their study of liquid samples with an external beam, employed the program SKEWGAUS[87] which is capable of performing suitable multiplet fits to unresolved peaks. Lien et al.,[88] in their analysis of water samples, used an IBM 1800 computer off-line to analyze the data. Their program also fitted Gaussians to the X-ray peaks, but employed a quadratic representation of the background. Unfortunately, no details of the degree of sophistication of the program are given.

Willis and Walter[89] report a semiautomatic program, TRACE, based on a nuclear physics routine, GAUSSN, which also employs a Gaussian function to represent the X-ray line shapes after removal of the background. The background is obtained by fitting a polynomial to selected data points selected by the operator with a light pen. The polynomial and the Gaussians are then used to define an initial fitting function which is parameterized in terms of background coefficients, peak amplitudes, peak positions, and widths. The subroutine CURFIT (Bevington[90]), then performs a least squares fit to the fitting function which combines a linearization of the fitting function with a gradient type search to minimize χ^2. The present form of the program is limited to fitting 22 K-line elements and 5 L-line elements, although others can be included via a card input. The main limitation is that only 13 elements can be handled at any one time so that complex spectra require division into selected regions. The authors report that the background fitting procedure requires improvement and that they are investigating ways by which the operator participation can be reduced. A semiautomatic program is also employed by Hasselmann et al.[91] in their analysis of biological tissues. This program, SESAM-X, is run on a small off-line computer with a minimum of operator interaction. A Gaussian function is again employed to fit the X-ray lines of 35 elements up to a maximum of 160 peaks. Only one free parameter is needed for each element since normalization factors, X-ray energies, and relative intensities are previously stored in the computer. The background contribution to the spectrum is obtained from previously experimentally determined background spectra for a variety of different matrices. The normalization to which the background functions are fitted is again accomplished by means of a light pen.

Van Espen et al.[92] describe a Fortran program, AXIL, designed to run on a PDP 11/45 system for the analysis of low energy X-ray spectra obtained using tube-excited X-ray fluorescence, which is readily applicable to spectra obtained by electron- or proton-induced emission. In common with several other programs a simple Gaussian is used to represent the response function of the full energy X-ray peak, while the background is represented by a suitable polynomial. The program incorporates an iterative nonlinear least squares fitting routine which minimizes χ^2 in a similar manner to that employed by Willis and Walter.[89] Optional peak position, resolution, and spectral constraints are

available to the operator. This ensures that the peak positions and resolutions are in agreement with the calibration expressions. Their use has the advantage that it leads to a reduction in the memory size required and the speed of computation. The spectra are analyzed in energy sections typically 5 keV wide. The authors report that work is in progress to obtain an improved instrumental response function to remove the systematic errors which arise in extreme situations.

A fully automatic computer program, RACE, is employed by Cahill[80] for his data reduction of environmental samples. The analysis is performed on a PDP 15/40 computer while simultaneously new data is being accumulated. The program occupies 14K words of memory and covers all possible elements. Background is again obtained from an experimental run on a blank and normalized to the minima in the data. Any small residual background is fitted by a parameterization. After subtraction of the background a correlation technique employing a Gaussian of fixed width is employed to identify the peaks. In a similar fashion the program inspects the spectra for the presence of any multiplets and determines their order. Cahill[80] stresses the importance of including, in any fully automatic system, a subroutine which draws the attention of the operator to any problems of assignment encountered. Rickey et al.[58] also employ a fully automatic data evaluation program, run on a PDP-15 computer, which is capable of identifying all possible elements on-line while the next set of data is accumulated, typically 15 min. The program differs from that of Cahill[80] in that the background is not obtained from blanks. This is because the samples to be analyzed vary in thickness and content, thus introducing significant absorption effects which distort the background and in addition alter the relative intensities of the characteristic peaks. The background contribution is determined by reference to the physical processes that produce it, similar to the initial approach of Kaufmann and Akselsson.[93] The high energy background >15 keV, due to proton bremsstrahlung and Compton scattered gamma rays, is directly determined from the data and subtracted from the low energy region. This leaves only the electron bremsstrahlung in the low energy region of the form given by Folkmann,[4] $I = AE_x^{-b}$, which is adequately represented by a low order polynomial or a series of straight-line segments. Adopting this approach an adequate representation of the true background is readily obtained by folding in the absorption and detector efficiency. A fitting function employing up to 5 Gaussians with low energy tails is then least squares fitted to the data to obtain the peaks. The program routine is capable of handling the silicon escape peaks from intense lines and pulse pile up, and draws the operator's attention to any problems that occur during the analysis.

Kaufmann et al.[94] report on the improvements made in the computer code REX. Details of the earlier versions have been discussed by Kaufmann and Akselsson[93] and Kaufmann et al.,[95] and are based on expressing the background in a way which reflects the physical processes involved. Since the modeling of the background on the physical processes is not without its difficulties, and in order to speed up the process, the latest version employs empirical expressions which represent the background adequately. The peaks are represented by the X-ray line shape convoluted with a Gaussian detector response. A nonlinear least squares fit is then made to all the model parameters simultaneously. This approach has been found to handle elemental interferences very satisfactorily. The program occupies 42K of memory of a Dattacraft 6024/3 computer and processes a spectrum in under 180 sec. The authors plan to refine the model to include the silicon escape peaks and any possible small radiative Auger emissions.

An alternative approach is described by Lecomte et al.[65] in their study of trace elements in serum samples. The concentration of the elements present in the sample is obtained by comparison with a known reference element, such as yttrium, used as an internal standard. The analysis of the spectra is done on-line using a small 32K CDC 3100 computer. The program is semiautomatic in that the elements sought, the internal standard

concentration, and the maximum number of iterations required, have to be declared. The procedure employs standard reference spectra recorded under controlled experimental conditions. The program strips off peaks from the spectrum till only the desired elements are left. From the resulting data the scale factors of the required elements are determined using a linear representation of the background at high energies and a parabolic function at low energies over a region three times the full width at half maximum of the peak of interest. A precision of 1% is readily obtained with three or four iterations on well-separated peaks, while more iterations are required for complex multiplets. The main limitation of the program is that it cannot accommodate variations in experimental conditions which may well have to be optimized differently for the analysis of different elements.

Nass et al.[96] have developed a program which is virtually automatic for all but the most complex of spectra. The data is first smoothed, as described by Yule,[97] using a unit area Gaussian as the smoothing function, the width of which was chosen to represent the detectors energy response. The smoothed data are differentiated and appropriate minima selected to which the background is fitted. A least squares fit is employed to obtain a suitable fitting function above 4 keV, while below a 3rd degree spline fit is used. The background subtracted data are smoothed again with a Gaussian and differentiated to locate peak positions. In regions of the spectrum where the peaks are not isolated the data are convoluted with a Gaussian of width W/2 and W/10, where W is the expected width, to identify the overlapping peaks. The authors report that the main limitation appears to be that peaks which are close to the background level are occasionally missed. A typical spectrum before and after computer evaluation is shown in Figure 17.

Clearly the goal of the PIXE analyst to have a very rapid, fully automated, computer-evaluated data analysis system which is capable of handling interferences, multiplets, and absorption, will soon be achieved.

IV. ELEMENTAL ANALYSIS

An elemental analysis of a sample is performed in order to obtain information on its elemental constituents. In many instances a straightforward qualitative analysis is all that is required and confirms the presence or absence of certain elements in the sample. The more comprehensive quantitative analysis in addition to identifying the elements present in the sample enables their quantities to be specified. For many analysts the ultimate aim is to detect and quantify the smallest amount of an element present in a given sample based on information produced characteristically by the elements of interest. As with all systems, competing processes generate undesired information which, from the view point of the analysis, is regarded as noise. The signal-to-noise ratio effectively determines the sensitivity of the method and ultimately defines the smallest quantity of an element of interest that can be detected.

A. Minimum Detection Limit

The minimum detection limit (MDL) for a given element may be defined as the minimum quantity of that element which must be present in the sample to yield a significant amount of signal above the noise to enable its identification and measurement. If the criterion is set such that a significant signal is taken as one which is one standard deviation above the background, then there is an 84% probability that the element is present in the sample. For a signal two standard deviations above background the probability is 97.7%, and for three standard deviations, 99.9%.

If a characteristic X-ray peak in a spectrum from an analyzed sample is positioned on a general background, as shown in Figure 18, then the total number of counts in the peak,

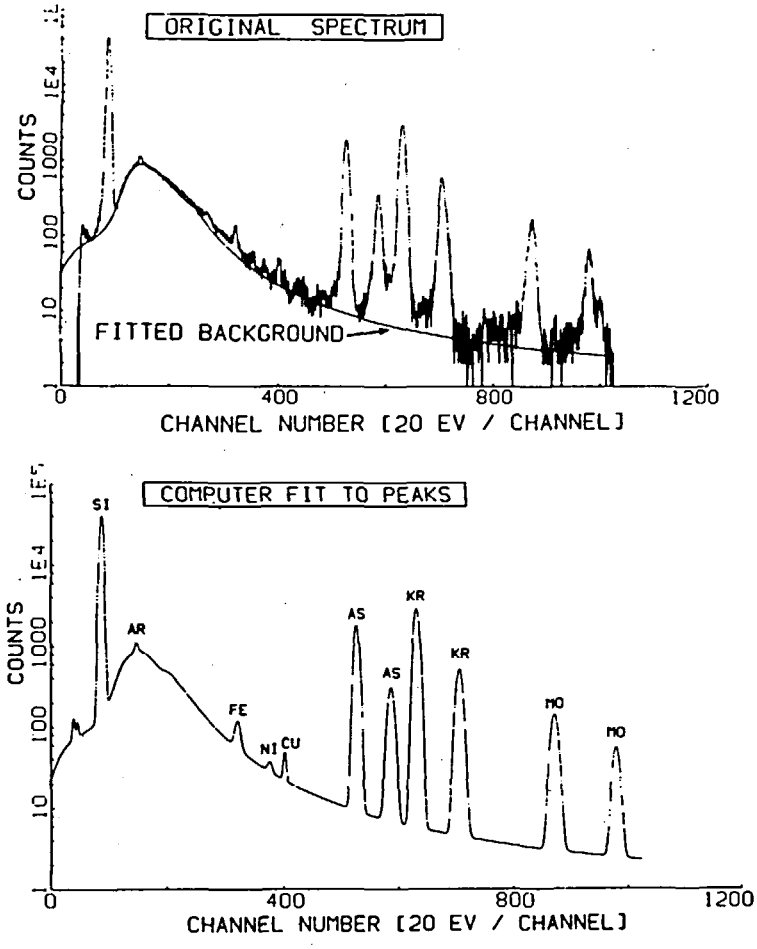

FIGURE 17. Typical original X-ray spectrum and computer evaluated spectrum. (From Nass, M. J., Lurio, A., and Ziegler, J. F., *Nucl. Instrum. Methods*, 154, 567 (1978). With permission.)

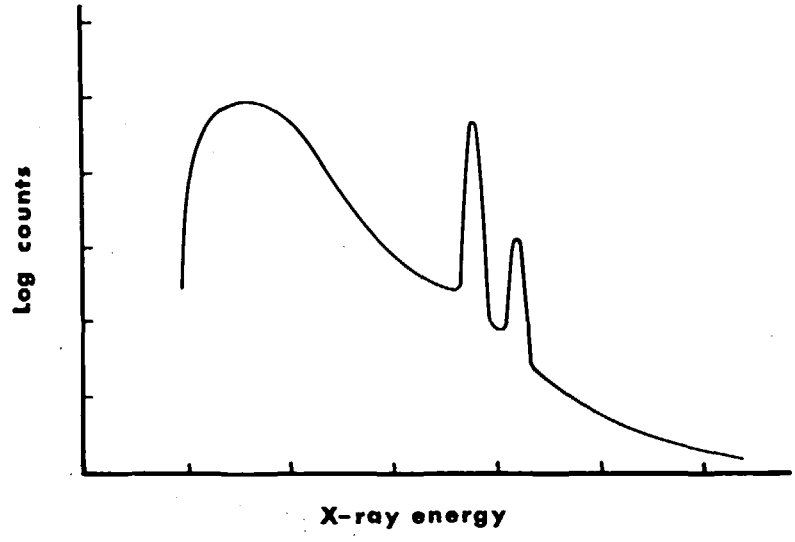

FIGURE 18. Characteristic X-ray peak and continuous background.

N_T, is equal to the background counts N_B plus the true peak count, N_o. The true K_α peak count, N_o, and its associated standard deviation, is given by

$$N_o = \left[N_T - N_B \right] \pm \sqrt{N_T + N_B} \qquad (6)$$

The standard definition of statistical significance as defined by the International Union of Pure and Applied Physics is that $N_o \geq 3\sqrt{N_B}$, that is the peak must be at least as large as the uncertainty in the background. Cahill[80] has shown that the above assumption leads to the following expression for the minimum detectable areal density of a thin sample $(\rho t)_s$ mounted on a backing of areal density $(\rho t)_B$;

$$MDL = \frac{3}{(n_o)^{1/2}} \left[\left(\frac{A_Z}{N_A \sigma_X \, d\Omega \, \epsilon} \right)^2 \left(\frac{N_A \sigma_{BX} \, d\Omega \, \epsilon}{A_B} \right) \right]^{1/2} \left[(\rho t)_B + (\rho t)_s \right]^{1/2} \qquad (7)$$

where A_Z and A_B are the mass numbers of the sample and the backing respectively, σ_X and σ_{BX} the X-ray production cross-sections for the sample and backing, ϵ the detector efficiency, $d\Omega$ the detector solid angle, N_A Avogadro's number, and n_o the number of protons incident on the sample. A detailed analysis of the optimization of this expression has been reported by Cahill[80] to obtain the most realistic minimum detectable level for a given system and sample. The variation of the MDL to changes in the parameters in Equation 7 is given in Table 3 which is reproduced from Cahill.[80]

B. Precision and Accuracy

The accuracy of a measurement relates to how close the measured value agrees with the true value. In practice, however, the true value is seldom known. It is only through statistical treatment of data that a "true" value is estimated from the measurements, which themselves are subject to uncertainties. Basically there are two kinds of uncertainty or error, random and systematic. Random errors are fundamental in the sense that they are an intrinsic property of all measurement processes and evolve from the fundamental properties of the instruments employed in the measurements. Systematic errors arise due to errors in standard values (values used in calculations but not measured in the specific experiment), instrumental error (e.g., incorrect calibration of a detector), indeed, any error which is constant for a specific experimental configuration. The estimate of the uncertainty arising due to the random error is known as the precision of the measurement and the error due to systematic effects is known as the accuracy of the measurement. It is often very difficult to identify and eliminate systematic uncertainties associated with a particular experiment, however, the use of well-characterized standard materials such as those obtained from NBS are very valuable in revealing systematic uncertainties. The accuracy and reproducibility depends to a large extent on the care with which the initial system is set up and calibrated and on careful sample preparation. In this respect, interlaboratory comparisons of results obtained from identical samples are particularly useful.

C. Sample Integrity

In preparing samples care must be taken to ensure that the constituent elements are uniformly distributed throughout the samples, otherwise reproducibility of results between samples will not be possible. Many biological samples are heterogeneous in nature and consequently cannot be analyzed directly without adequate preparation. In

Table 3
VARIATION OF MINIMUM DETECTABLE LIMIT, $(\rho t)_{x,min}$

	Variation
Detector	
Solid Angle ($d\Omega$)	$(d\Omega)^{-1/2}$
Energy Resolution (ΔE)	$(\Delta E)^{1/2}$
Count Rate (R)	$(R)^{-1/2}$
Target	
Backing Thickness $(\rho t)_B$	$[(\rho t)_B + (\rho t)_x]^{1/2}$
Characteristic Cross Section (σ_x)	$(\sigma_x)^{-1}$
Backing Cross Section (σ_{Bx})	$(\sigma_{Bx})^{1/2}$
Ion Beam	
Ion Velocity	Optimum at ~ 0.1 c
Ion Charge (Z_i)	$(Z_i)^{-1/2}$
Ion Integrated Current (Q)	$(Q)^{-1/2}$
General	
Time, T	$(T)^{-1/2}$

From Cahill, T. A., Ion-excited X-ray analysis of environmental samples, in *New Uses of Ion Accelerators*, Ziegler, J. F., Ed., Plenum Press, New York, 1975, 1. (With permission.)

addition, sufficient primary sample must be taken from which the samples are prepared to ensure that they are representative of the bulk. For example, NBS recommend that when preparing samples from NBS bovine liver at least 250 mg are used to ensure that it is representative of the bulk. For semithick samples, the uniformity of the sample thickness must be maintained if the energy loss of protons and the absorption of X-rays in the sample are to be reproducible. Finally, if the sample contains volatile materials or is nonthermal conducting the sample may lose its integrity due to heating effects. Willis et al.[98] have reported that in the case of bovine liver concentration effects occur at beam currents as low as 40 nA due to selective vaporization of the organic matrix.

D. Beam Uniformity and Size

The size of the proton beam striking the sample and its uniformity can be controlled by appropriate techniques to suit the experimental arrangement concerned. A large area beam has the advantage that it allows the local power density to be reduced without loss of sensitivity, and thus reduces target heating. A uniform beam compensates for any nonuniformity of the sample, provided the irradiated area is representative of the sample. A convenient way of establishing the requirements for beam size and uniformity is to consider a specific analytical situation, such as the analysis of a thin sample using a calibration standard. An expression for the areal density of the sample, $(\rho t)_s$ and its mass, M_s, can be obtained from the X-ray yield of the sample, Y_s, and of the standard, Y_{st}, in terms of the areal density of the standard $(\rho t)_{st}$. The actual expression obtained depends upon the size of the proton beam in relation to the size of the sample and standard. The more usual arrangements for beam size, sample, and standard size, are given in Table 4, together with the appropriate expressions for evaluating the areal density of the sample and its mass, in terms of the standard containing a known mass, M_{st}, of the element of interest, when standard and sample are irradiated with a fixed number of protons. If the size of the beam spot at the sample position is uncertain, or likely to alter from one irradiation to the next, then only configurations (i) and (ii) will yield reproducible results. If the sample is known to be uniform then it is not necessary to have a uniform beam,

Table 4
EXPRESSIONS FOR THE AREAL DENSITY OF THE SAMPLE AND ITS MASS FOR THE MOST USUAL ARRANGEMENTS OF BEAM SIZE, SAMPLE, AND STANDARD SIZE

	Relative size compared with beam size of			
	Standard	Sample	Areal density of sample, $(\rho t)_s$	Mass of sample, M_s
(i)	Smaller	Smaller	$(\rho t)_{st}\,(Y_s/Y_{st})\,(dS_{st}/dS_s)$	$M_{st}\,(Y_s/Y_{st})$
(ii)	Larger	Larger	$(\rho t)_{st}\,(Y_s/Y_{st})$	$M_{st}\,(Y_s/Y_{st})\,(dS_s/dS_{st})$
(iii)	Smaller	Larger	$(\rho t)_{st}\,(Y_s/Y_{st})\,(dS_{st}/dS_B)$	$M_{st}\,(Y_s/Y_{st})\,(dS_s/dS_B)$
(iv)	Larger	Smaller	$(\rho t)_{st}\,(Y_s/Y_{st})\,(dS_B/dS_s)$	$M_{st}\,(Y_s/Y_{st})\,(dS_B/dS_{st})$

Note: dS_s = area of sample, dS_{st} = area of standard and dS_B = area of beam.

however, the uniformity of the sample should always be suspect, and an attempt made to make the beam as uniform as possible, using one of the techniques previously discussed.

E. Sample and Detector Positions

With regard to the sample position the configuration often employed is to have the sample mounted at 45° to the incoming proton beam. In order to obtain reproducible results from successive samples it is important that the samples be brought to the same position each time. In the case of thin samples positioned as above, the thickness seen by the proton beam is $t\sqrt{2}$. Clearly any change in angular position will change the X-ray yield resulting in a loss of reproducibility, a 1° change in angle, for example, changes the yield by approximately 2%. The effect on the X-ray yield of tilting the sample, i.e., not being positioned in the vertical plane, is much less pronounced. In the case of infinitely thick samples it is not the production of X-rays that changes but the absorption of the X-rays in the matrix of the sample. Thus, changes are dependent on the X-ray energies and the nature of the sample matrix.

With the configuration described the detector is normally placed at the position of specular reflection, i.e., 90° to the incident beam. This has the advantage that it simplifies calculations involving integration of the thick target yield, and it was initially thought, by Folkmann et al.,[99] that any anisotropy associated with the background was too small to be exploited. More recently, Ishii et al.[100] have demonstrated that at angles in excess of 90° the background intensity is minimized, thus enhancing sensitivity usefully by a factor of nearly two.

F. General Filters

Many samples requiring analysis are abundant in the light elements which may not be of interest. Under these circumstances, it is desirable to reduce their contribution to the X-ray spectrum by placing a thin filter between the sample and detector, which preferentially absorbs the X-rays from the light elements. Cahill[80] employs a 76 mg/cm^2 CH_2 filter which transmits about 50% of the iron K_α lines and results in a sensitivity of essentially zero for elements below calcium. Problems can occur with sample analysis when medium and heavy elements present in small amounts need to be detected with maximum sensitivity against a dominant contribution from the light elements which must also be measured. Normally this requires the sample to be irradiated twice — measurements being taken with and without the normal filter. Cahill[80] describes a novel approach to this problem and employs a filter of preselected thickness which is pierced by a small hole to allow a fraction of the light elements through to the detector. The

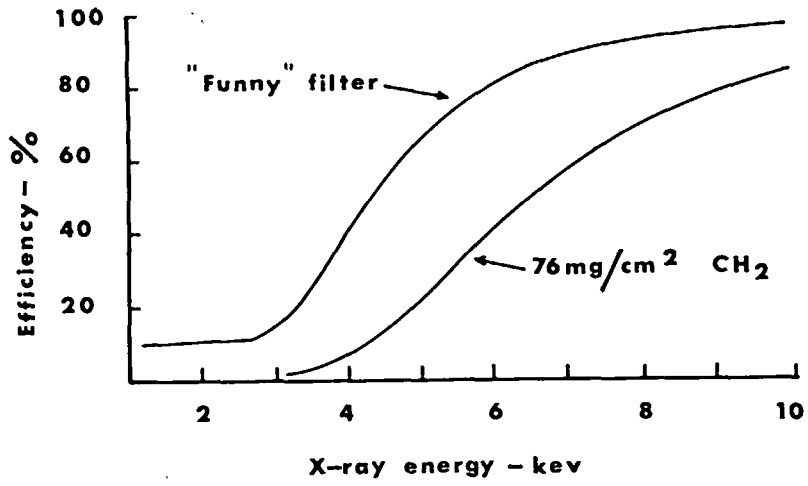

FIGURE 19. Comparison of the efficiency of a CH_2 filter and a filter pierced by a small hole. (From Cahill, T. A., *New Uses of Ion Accelerators,* Plenum Press, New York, 1975, 1. With permission.)

efficiency for this type of filter compared to the conventional CH_2 filter is shown in Figure 19 which is taken from the work of Cahill.[80] The advantages of this system are that only one analysis run is necessary, and a gain in sensitivity for the medium and heavy elements is obtained, thus permitting shorter analysis times.

V. THIN SAMPLES

Thin samples are defined as those in which (a) the energy loss of the incident particle is negligible, so that the X-ray production cross-section which is energy dependent, can be taken as sensibly constant throughout the sample, and (b) the absorption of X-rays, produced from the elements of interest, is negligible in the sample matrix. In the case of thin metallic samples X-ray absorption is the dominant criterion which determines the thickness and thin samples have areal densities typically 20 to 100 $\mu g/cm^2$. For biological samples the variation of cross-section with energy determines the thickness, and, thin biological samples are typically 1 mg/cm^2 thick which is equivalent to approximately 10 μm. Campbell[101] has proposed that a thin specimen criterion be employed (T.S.C.) for biological samples in which the effective cross-section is taken as the cross-section associated with the mean energy of the protons in the sample. For example, a 2.5 MeV proton beam loses an energy of 0.12 MeV in passing through a 1 mg/cm^2 thick carbon target. Assuming that the element of interest was iron, its X-ray production cross-section decreases by some 12% for this energy change. According to Campbell the effective cross-section is therefore taken as 6% less than the X-ray production cross-section at the initial energy of the protons.

Folkmann et al.[99] have made a detailed theoretical and experimental study of the background that arises from thin samples, from which they have estimated the sensitivity as a function of atomic number, based on the observation of K X-rays, for a range of proton energies. They employed the criterion that the signal-to-noise ratio must be equal to or greater than one for positive identification, within a window width equal to the peak width. Their results for the sensitivity achievable using a thin carbon backing are reproduced in Figure 20, and show that the optimum sensitivity occurs at different energies for different atomic numbers. Subsequently this approach was extended to thick

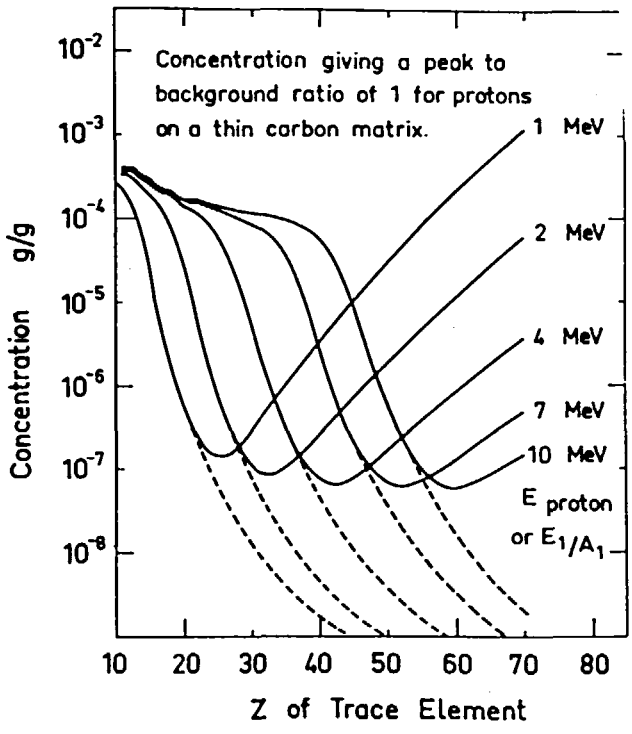

FIGURE 20. Calculated minimum concentration of trace elements detectable for protons on a thin carbon matrix, based on a signal to noise ratio of one. (From Folkmann, F., Gaarde, C., Huus, T., and Kemp, K., *Nucl. Instrum. Methods*, 116, 487 (1974). With permission.)

homogeneous targets and the results compared with those for thin targets, as shown in Figure 21 (reproduced from Folkmann[102]).

Thin samples such as those discussed above require some sort of support such as Mylar®, formvar or a polycarbonate membrane, and prior to their deposition on such backing materials the samples often require special preparation techniques. Since the beam passes through the backing material as well as the sample a very careful measurement of the elements present in the target supporting material must be made. The preparation of suitable samples can conveniently be discussed under the headings of direct preparation techniques and enrichment methods. In the direct preparation, the sample undergoes a minimum of physical manipulation and includes solution deposition, sectioning, and direct irradiation without preparation.

A. Direct Preparation

1. Solution Deposition

Liquid samples, such as water, urine, blood, serum, and other body fluids, are usually deposited as a drop from an hypodermic syringe or micropipette onto the thin backing material and allowed to dry.[1,2,13,63] The prepared sample is then analyzed in the normal manner. Though this is a simple and widely used method for such samples there is some evidence that samples prepared in this manner are not always homogeneous, in that the trace elements are deposited differently along the radii. In addition, blood samples and suspensions with fibrous tissues deposited in this way tend to deform the thin backing materials when they dry.

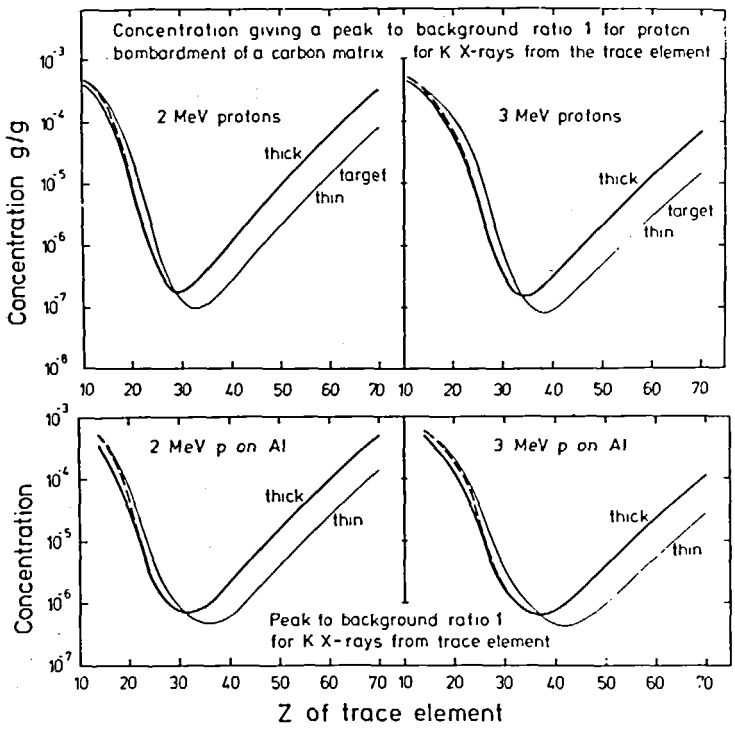

FIGURE 21. *Calculated minimum concentration of trace elements detectable* for protons on thick and thin targets. The effect of absorption in the matrix for an angle of 45° is shown by the dotted line. (From Folkmann, F., *Ion Beam Surface Layer Analysis, II,* Plenum Press, New York, 1976, 747. With permission.)

A multidrop technique is reported by Camp et al.[103] which involves depositing 220 $\mu\ell$ of solution onto a support 10 to 15 $\mu\ell$ at a time, just enough to wet the entire surface. A standard solution containing nine elements was employed and analyzed by a variety of techniques at a number of laboratories. The K, V, Mn, Fe, and Cu composition was found to be homogeneous with a standard deviation of less than 3%. An alternative approach employed by Baum et al.[104] involves the use of 37 capillary tubes which deposit their contents simultaneously onto a backing material. The samples are then freeze-dried to prevent differential migration of the elements along the radii. As the tubes are not disposable, great care must be taken to avoid contaminations. Kivits et al.[105] describe a method for the preparation of samples from aqueous solutions by rapidly depositing the solutions onto a fast rotating foil. Selectron foils of areal density 5 mg/cm^2 were rotated at 18,000 rpm and the aqueous solution, typically 50 $\mu\ell$, deposited from a microdispenser as rapidly as possible, in less than 0.2 sec, and then allowed to air-dry at room temperature. An equal volume of ethanol was added to the aqueous solutions in order to obtain a suitably reproducibly uniform deposit. Uniformity and homogeneity of the samples was measured along the radii of the samples using a 2-mm diameter proton beam. A nonuniformity of $<6\%$ and a nonhomogeneity of <1 to 2% was observed, indicating that migration along the radius does not occur in this case. Jolly and White[11] have described a method for the preparation of thin samples from biological, environmental, and other materials in the form of suspensions. The initial samples were first broken into microscopic sizes by a variety of methods and then made into a colloidal solution. These solutions were then sprayed uniformly onto a suitable backing material using a nebulizer

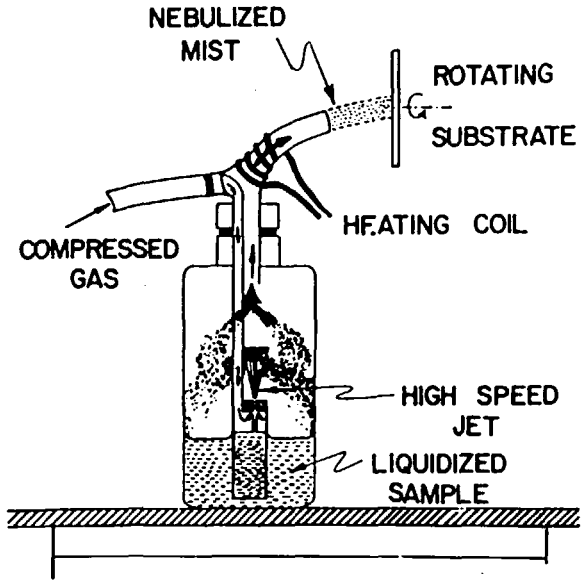

FIGURE 22. Schematic diagram of a nebulizer for depositing a thin film of dissolved or suspended matter onto a backing. (From Jolly, R. K., and White, H. B., *Nucl. Instrum. Methods*, 97, 103 (1971). With permission.)

(Figure 22). Compressed gas is applied to the input of the nebulizer resulting in a mist of very fine droplets at the nozzle which is directed at the backing material. The droplets are very often so fine that they cannot be seen by the unaided eye even when illuminated by a very strong light. Very fine particles of micron size can be deposited uniformly by this method to produce samples suitable for analysis of thicknesses 10 to 1000 $\mu g/cm^2$.

2. Sectioning with a Microtome

Thin sections of tissue can be cut with a microtome by either embedding the tissue in an hardening agent, such as paraffin wax, or by freezing the primary material and then sectioning it, using a cryostat microtome operating at a temperature of −20° C. Sections such as these can then be analyzed as a self-supporting sample attached to a suitable holder with a small amount of adhesive, or mounted on a suitable thin backing material. Kemp et al.[106] have studied self-supporting sections of liver, and Walter et al.[13] have analyzed thin sections of animal tissue. Campbell et al.[107] have analyzed tissue slices of 10 μm thickness and 5 to 10 mm diameter mounted on carbon backings. Hasselmann et al.[91] have analyzed frozen sections of liver and spleen of about 10 μm thickness and also paraffin-embedded liver tissue.

From the point of view of contamination the cryostat microtome is to be preferred to the embedding of tissue in a hardening agent, since it is likely that even when the hardening agent is dissolved prior to mounting the samples that contamination of the tissue could occur. It has also been observed that very small specimens obtained by microtome slicing are often unrepresentative of the bulk material and thus care must be exercised in interpreting the data.

3. Direct Irradiation without Preparation

If the specimen to be analyzed is of suitable thickness then it can be used as a sample directly without any manipulation. Air particulate deposits as obtained from air

sampling systems are ideally suited to direct irradiation. Hair is also suited to this approach. Jolly et al.[108] and Valkovic et al.[109] have studied hair directly and determined the concentration of elements as a function of distance along the hair.

B. Enrichment Methods

These methods are employed firstly for the analysis of elements which are available in very low concentrations of less than 0.1 to 0.2 ppm and secondly to obtain homogeneous samples from nonhomogeneous specimens. Methods available include freeze drying, dry ashing, wet ashing, successive evaporation, and vacuum filtration.

1. Freeze-Drying or Lyophilization

In freeze drying the tissue or organic substance is frozen and then the freezing chamber is evacuated and pumped for a relatively long period of time to sublimize the ice. This leaves a solid residue which can be thoroughly powdered to ensure uniformity of elements throughout. Campbell[101] found that freeze drying enabled the mass of the sample to be concentrated by a factor of 5. Campbell et al.[107] also pointed out that 1 mg of sample is unlikely to be sufficiently homogeneous to be representative of the bulk material, a fact substantiated by their measurements on small samples of SRM 1571 (orchard leaves) and powdered basalt.

2. Ashing

The purpose of the ashing process is to increase the elemental concentration of elements of intermediate atomic number by the removal of the low atomic number elements, such as hydrogen, carbon, nitrogen, and oxygen, which are the major constituents of biological materials. The process also results in a homogeneous sample. Dry ashing or dry oxidation can be done either at low or high temperatures. Ashed samples of plant tissue, bone, soft animal tissue, blood, and milk have been prepared by Rudolph et al.,[110] Bearse et al.,[111] and Mangelson et al.[112] Gorsuch,[113] in his comprehensive monograph "The Destruction of Organic Matter," advises that dry ashing should be avoided unless it is absolutely necessary, as volatile elements are frequently lost in the process.

Wet ashing or digestion has been used successfully by several workers. In this procedure about 300 mg of sample is digested with a suitable digestion agent, with or without heating. The wet ashing agent reduces the biological material to a homogeneous solution of oxidized material from which samples for analysis can be prepared. Walter et al.[114] have found that a mixture of concentrated nitric acid and sulfuric acid in the ratio 2 to 1 is necessary to obtain a clear solution for the digestion of human lung. It should be noted, however, that sulfuric acid has a very high boiling point and evaporation to dryness of a solution containing sulfuric acid can present problems. Nielson[115] has used tetramethylammonium hydroxide as a basic agent for wet ashing, but found that much of the original material was not completely oxidized. Campbell et al.[107] have also employed the wet digestion method, dissolving 0.25 g of initial material in ultra pure nitric acid. One or two drops of the acidic solutions were then deposited on 20 $\mu g/cm^2$ carbon foils and evaporated to dryness. Digestion was done in "polyvials" (Olympic Plastics Inc.) or in Uni-Seal high-pressure decomposition vessels (Uniseals Decomposition Vessels, Ltd., Haifa, Israel). The decomposition vessels have the advantage that the digestion can take place under enhanced pressure, with no loss of volatile components.

Naturally, care must be taken when handling wet ashing agents and the digestion should be carried out in a good fume cupboard to exhaust the toxic gases which are released during the oxidation processes. If samples are to be prepared by depositing one or two drops of solution onto foils and evaporating to dryness then the use of sulfuric acid

as one of the digesting acids should be avoided as its high boiling point makes evaporation to dryness difficult.

3. Vacuum Filtration

Rickey et al.[116] have successfully employed the technique of vapor filtration to prepare suitable targets from aqueous samples. The procedure for sample preparation enables extremely small quantities of material to be recovered and minimizes contamination problems. A schematic diagram of their vapor filtration apparatus is shown in Figure 23.* The water solution, typically 30 mℓ, from which the enriched target is to be prepared, is enclosed in the vertical tube mounted on a suitable membrane which in turn is supported by a porous polyethylene disc. The pressure on the vacuum side of the membrane is kept below 4 torr, since at these pressures the water exists only in the vapor phase. Continuous pumping for 3 days was necessary to pass the 30 mℓ water samples through the vapor filter. Although the system works well for water solutions and solutions containing 1.5 mℓ concentrated nitric acid per liter of water, solutions prepared from other acids and larger concentrations were found difficult to process.

4. Other Techniques

For the analysis of natural water Lochmüller et al.[117] employed ion exchange media to obtain enriched samples. Electrodialysis membranes were impregnated with a suitable cation exchange resin and placed into the water to be sampled. The metal ions in the water are absorbed onto the membranes over a period of several days due to the long equilibration time. After rinsing and drying, the membranes were used directly as targets for proton-induced X-ray emission analysis. The studies undertaken showed that for certain elements of environmental interest sensitivities of the order of 1 ppb were possible employing this procedure.

An alternative approach for preparing enriched samples from liquids has been investigated by Akselsson and Johansson.[34] Rainwater and seawater in 1 mℓ samples were employed to which a suitable complexing agent was added, such as 8-hydroxyquinoline. The metal complexes formed were then absorbed onto activated carbon which was subsequently collected onto a filter. The authors chose to analyze the carbon in the form of a pellet and achieved a detection limit of the order of 1 ppb for the 1 mℓ samples.

C. Analysis of Thin Samples

In order to establish the relationship between the X-ray yield for an element and its concentration in a thin sample consider the irradiation of a thin sample, thickness t, by a parallel beam of protons of fixed energy E_p. The X-ray yield, Y, is given by the usual expression

$$Y = n_o \, N \, \sigma_x \, t \qquad (8)$$

where n_o is the number of protons incident on the sample, N is the number of atoms of the element of interest contained per unit volume in the sample, and σ_x is the X-ray production cross section for the element of interest. The number of atoms of the element of interest per unit area, N t, of the sample can be obtained from Equation 8 and is given by

$$N\,t = \frac{Y}{n_o \, \sigma_x} . \qquad (9)$$

* Process and device protected by U.S. Patent 4,108,718 held by Purdue Research Foundation, West Lafayette, Ind., 47907.

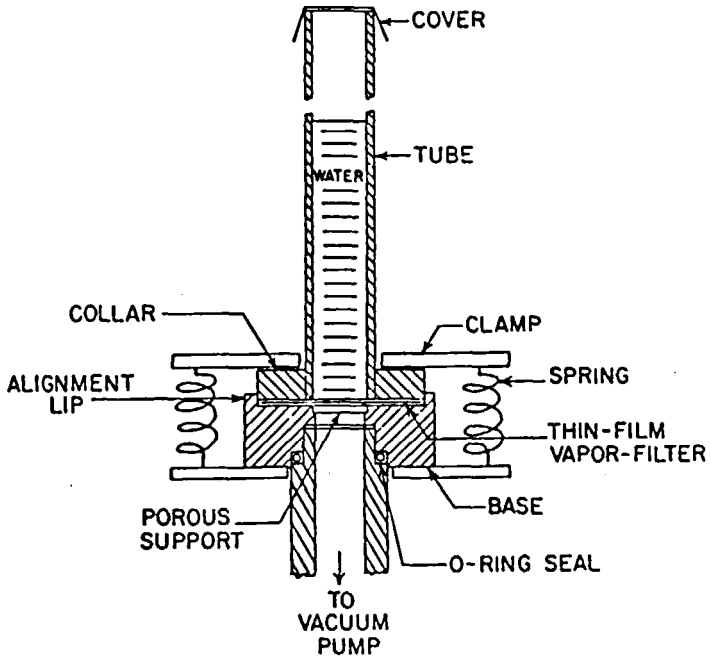

FIGURE 23. Vapor filtration apparatus. (From Rickey, F. A., Mueller, K. A., Simms, P. C., and Michael, B. D., Sample preparation for multi-elemental analysis of water, in *X-ray Fluorescence Analysis of Environmental Samples,* Dzubay, T. G., Ed., Ann Arbor Sci., Ann Arbor, Mich., 1977, 134; Simms, P. C. and Rickey, F. A., Purdue University, West Lafayette. Ind., 1978. Protected by U.S. Patent 4,108,718 held by Purdue Research Foundation, West Lafayette, Ind., 47907. With permission.)

Since the weight of one atom is A/N_A, where A is the mass number of the element and N_A Avagadro's number, the mass per unit area of the sample is obtained by multiplying Equation 9 by A/N_A. Hence, the mass/unit area of the element of interest in the sample, usually denoted (ρt) is given by

$$(\rho t) = \frac{Y\,A}{n_o\,N_A\,\sigma_x} \tag{10}$$

where ρ is the density of the element of interest *in the sample.*

For X-radiation detected in a solid angle $d\Omega$ by a detector of efficiency ϵ, following partial absorption of the X-rays in the scattering chamber exit window and the air path between the window and detector, Equation 10 becomes

$$(\rho t) = \frac{Y_x}{n_o}\left[\frac{A}{N_A\,d\Omega\,\sigma_\theta\,\epsilon\,e^{-\Sigma\mu_i x_i}}\right] \tag{11}$$

where Y_x = the number of detected X-rays, σ_θ = cross-section for X-ray production per unit solid angle at an angle θ, corresponding to the angle of observation of the X-rays, $e^{-\Sigma\mu_i x_i}$ = absorption of X-rays in the chamber windows, air path to the detector and detector window, μ_i = linear absorption coefficient for absorber i, X_i = thickness of absorber i. For a fixed proton energy, element of interest, X-ray transition, and geometry the bracket in Equation 11 is constant and hence the areal density is given by

$$(\rho t) = \frac{Y_x}{n_o} K(Z) \qquad (12)$$

where K (Z) is a constant which can be evaluated for each element of interest. Thus a determination of the X-ray yield, Y_x, for a fixed number of protons, n_o, enables the areal density, (ρt) of the element of interest to be determined.

D. System Calibration

Central to all analytical techniques is the problem of converting qualitative results into quantitative information concerning the elements present in the sample under investigation. In common with other analytical techniques a number of possibilities exist which include:

1. Use of internal standard.
2. Calibration using standard reference materials.
3. Calibration using thin spectroscopically pure samples.
4. Use of published cross section data.
5. Use of theoretical values for cross sections.

These procedures are referred to as system calibration. In order to validate the system it is necessary to calibrate the system by more than one method, as pointed out by Cahill,[80] who has discussed the first four of these procedures in some detail.

1. Internal Standards

The first step in this procedure is to prepare a thin sample of known elemental composition and bombard it with protons of a suitable energy E for sufficient time to accumulate a statistically meaningful number of counts in each detected X-ray peak. The number of detected X-rays appropriate to each element present is then normalized by the known elemental composition to obtain the relative X-ray yield per atom. These normalized yields are then plotted as a function of the atomic number Z of the elements at the selected energy, and employed as a system reference for the determination of the elemental composition of the unknown sample.

The unknown sample is doped or "spiked" with an element of known amount which should be small enough not to change the concentration of the other elements significantly. The dopant must be carefully selected so as not to be present in the original sample. The sample is then irradiated with protons and the resultant X-ray spectrum recorded. The number of detected X-rays for the dopant, Y_D, and the number for the element of interest, Y_Z, are given by equation 12, thus

$$(\rho t)_D = \frac{Y_D}{n_o} K(D) \qquad (13)$$

and

$$(\rho t)_Z = \frac{Y_Z}{n_o} K(Z) \qquad (14)$$

where D and Z refer to the dopant and the element of interest respectively. Hence,

$$(\rho t)_Z = (\rho t)_D \frac{Y_Z}{Y_D} \frac{K(Z)}{K(D)} \qquad (15)$$

Since the dopant and unknown element constitute the same sample the mass of the element M (Z) can be determined since

$$M(Z) = M(D)\frac{Y_Z}{Y_D}\frac{K(Z)}{K(D)} \qquad (16)$$

where the ratio $\frac{K(Z)}{K(D)}$ is obtained from the relative calibration curve.

2. Standard Reference Materials

Standard reference materials are now widely available from the National Bureau of Standards, Washington, D.C., and are being increasingly employed to evaluate analytical techniques, their precision and accuracy, and to enable the intercomparison of results from different laboratories. Standard reference materials contain known amounts of major and trace elements, the concentrations of which have been established by careful measurements using a variety of analytical techniques. The preparation and evaluation of two common standard reference materials, SRM-1571, Orchard Leaves, and SRM-1577, Bovine Liver, have been discussed by Lafleur.[118] The application of biological standard reference materials to elemental analysis and the problems relating to their use have been discussed in detail by Bowen.[119] For system calibration the standard reference material is made up into a sample and bombarded by the proton beam. The X-ray yield for each element of interest is then determined from which the K (Z) value of Equation 12 can be evaluated, thus providing the calibration of the system. Clearly the SRM should be chosen to be similar to the sample to be analyzed so as to obtain representative results. Cahill[80] points out, however, that sample matrix effects are inherent in this approach which can cause problems, particularly for elements where the X-ray energy is below 3 keV.

3. Spectroscopically Pure Samples

Spectroscopically pure thin samples of known areal density provide a direct approach to the evaluation of K (Z), Equation 12. Suitable thin samples in the form of single elements of 10 to 100 $\mu g/cm^2$ are readily available from a variety of sources with a quoted accuracy of $\pm 5\%$, deposited on mylar®, or polycarbonate supports. These are then bombarded by protons and the X-ray yield, Y_x, determined for a fixed number of protons, n_o, and hence K (Z) is determined. Sufficient samples are chosen to cover the elements of interest and a calibration curve drawn. Such a calibration curve, reproduced from Simms and Rickey,[120] is presented in Figure 24.

A complementary approach is to prepare thin samples in the laboratory from atomic absorption liquid solutions by depositing for example 1 mℓ of solution containing 100 μg of the element of interest onto a suitable backing material and evaporating to dryness. The K (Z) values are then determined in a manner similar to that described above. Simms and Rickey[120] employed 30 such samples to calibrate their system together with 33 commercially obtained thin samples, details of which are given in Table 5. Their comparison of the commercial samples and samples prepared from liquids by vapor filtration is reproduced in Figure 25. The observed yields are normalized by the values from a best fit to all the calibration points. Forty-six calibrators were employed to determine a best fit, the standard deviation of which was 3%. Twelve low calibrators were rejected and not included in the best fit determination.

A parallel approach has been reported by Akselsson et al.[121] for samples which are smaller than the proton-beam dimensions. The calibration is established by measuring the X-ray yield from a number of samples smaller than the beam and of accurately known

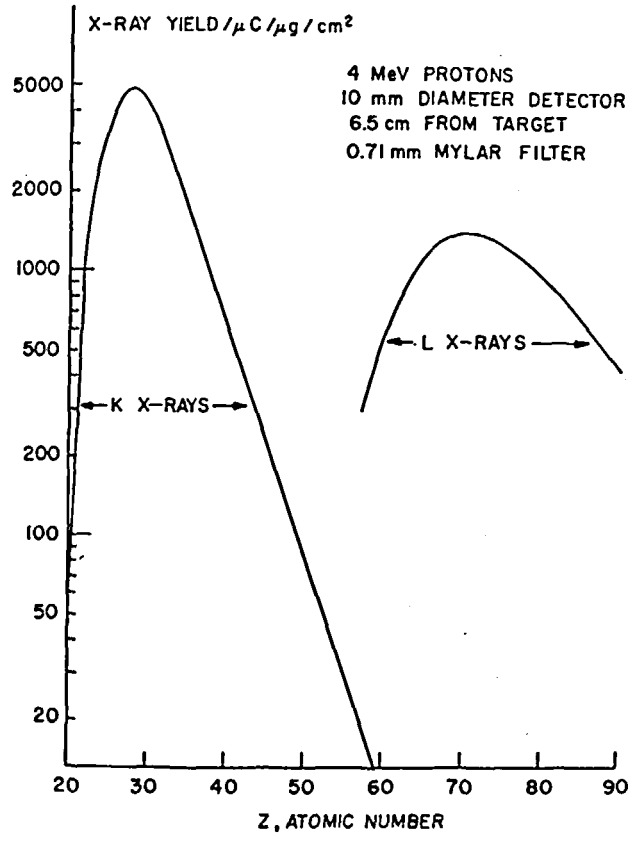

FIGURE 24. Calibration curve, giving the X-ray yield as a function of atomic number for a typical PIXE analysis system. (From Simms, P. C. and Rickey, F. A., Purdue University, West Lafayette, Ind., 1978. EPA-600/1-78-058. With permission.)

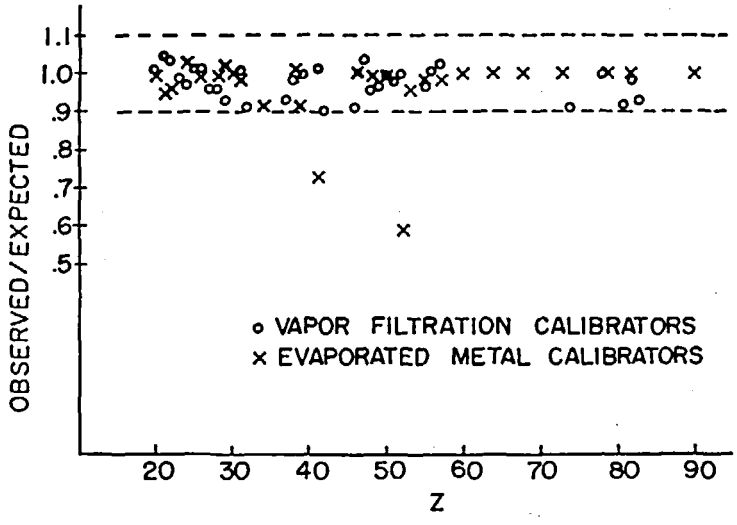

FIGURE 25. Comparison of vapor filtration calibrators and evaporated metal calibrators. (From Simms, P. C. and Rickey, F. A., Purdue University, West Lafayette, Ind., 1978. EPA-600/1-78-058. With permission.)

Table 5
ELEMENTS USED FOR X-RAY YIELD CALIBRATION

Element	Atomic number	Material used for evaporated film calibrators	Material used for vapor filtration calibrators
Aluminum	13	Al	
Silicon	14	SiO	
Sulfur	16	CuS	
Chlorine	17	NaCl	
Potassium	19	KCl	KCl
Calcium	20	CaF_2	$CaCO_3$
Scandium	21	Sc	$ScCl_3$
Titanium	22	Ti	Ti(in HCl)
Vanadium	23		V_2O_5
Chromium	24	Cr	$K_2Cr_2O_7$
Manganese	25		Mn(in HNO_3)
Iron	26	Fe	$FeCl_3$
Cobalt	27		Co(in HNO_3)
Nickel	28	Ni	Ni(in HNO_3)
Copper	29	Cu	CuO
Zinc	30	Zn	Zn(in HNO_3)
Gallium	31	GaP	$Ga(NO_3)_3$
Germanium	32	Ge	$(NH_4)_2GeF_6$
Selenium	34	Se	
Rubidium	37		RbCl
Strontium	38	SrF_2	$Sr(NO_3)_2$
Yttrium	39	Y	$Y(NO_3)_3$
Niobium	41	Nb_2O_3	
Molybdenum	42		Mo(in HNO_3 + HCl)
Palladium	46	Pd	$PdCl_2$
Silver	47		$AgNO_3$
Cadmium	48	Cd	Cd(in HNO_3)
Tin	50	Sn	Sn(in HCl)
Antimony	51		$SbCl_3$
Tellurium	52	Te	Na_2TeO_4
Iodine	53	CsI	
Cesium	55	CsI	
Barium	56		$BaCl_2$
Lanthanum	57	LaF_3	
Neodymium	60	NdF_3	
Gadolinium	64	Gd	
Erbium	68	Er	
Tantalum	73	Ta	
Tungsten	74		Na_2WO_4
Platinum	78		H_2PtCl_6
Gold	79	Au	
Thallium	81		Tl_2SO_4
Lead	82	Pb	Pb(in HNO_3)
Bismuth	83		Bi(in HNO_3)
Thorium	90	ThF_4	

From Simms, P. C. and Rickey, F. A., The Multielemental Analysis of Drinking Water Using proton-induced X-Ray Emission (PIXE); U.S. Environmental Protection Agency Report EPA-600/1-78-058. (With permission.)

mass. This calibration is then employed when evaluating the elemental composition of the unknown sample, and hence the various parameters that appear in K (Z) need not be known. The authors report an accuracy of the order of 10% for the calibration in terms of K X-rays.

4. Published Cross Section Data

The calibration factor K (Z) can be determined for each element and X-ray transition of interest by direct evaluation of the expression

$$K(Z)=\frac{A}{N_A\, d\Omega\, \sigma_\theta\, \epsilon\, e^{-\Sigma\mu_i x_i}} \tag{17}$$

The absorption of the emitted X-rays is calculated using the appropriate absorption coefficients which can be obtained from tabulations such as Storm and Israel[37] and Millar and Greening.[122] The solid angle $d\Omega$ subtended by the detector is calculated from a measurement of the target to detector aperture distance and the aperture diameter, or alternatively determined experimentally with the detector efficiency, which can be obtained as a function of energy as previously discussed. The X-ray production cross section can be obtained from the literature, an extensive survey of which has been made by Gardner and Gray.[41] Khan et al.[123] and Johansson and Johansson[31] have formulated empirical polynomial expressions based on experimental measurements which enables the cross sections to be readily evaluated. The usefulness of these equations lies in their ease of application and allows the extension of the data to other energies and atomic numbers. The polynomials of Khan et al.[123] are based on their experimental measurements of K X-ray ionization cross sections of several elements between Z = 20 and 50 in the proton energy range of 1 to 3 MeV. The equation for the ionization cross section, σ_I, requires only the input of the atomic number, Z, and the proton energy, E, and is given by

$$\begin{aligned}\ell n\, \sigma_I = {} & (41.46 - 37.32E + 8.448E^2) \\ & - (12.212 - 21.242E + 4.864E^2)\, \ell n\, Z \\ & - (0.0107 + 2.737E - 0.6551E^2)\, (\ell n\, Z)^2\end{aligned} \tag{18}$$

and is valid within the ranges $1.3 < E < 3$ MeV and $23 < Z < 50$. The equation differs by less than 3% from the Z-dependent equations, fitted to the experimental data, from which it was derived. The precision of the initial measurements of production cross sections, on which the equation is based, is reported to be less than 6% for the majority of elements studied. A polynomial in the format of the BEA universal curve is also given.

The polynomial of Johansson and Johansson[31] is based on the thin target measurements of several authors and is formulated according to the BEA universal form, and for a proton energy E in eV is given by

$$\ell n\, (\sigma_I U^2) = \sum_{n=o}^{5} b_n x^n \tag{19}$$

where $x = \ell n\, (E/\lambda U)$, λ is the ratio of the proton mass to electron mass, U is the appropriate ionization energy in eV, and the units of σ_I are 10^{-14} cm^2. The coefficients, b, are reproduced in Table 6. For the K cross sections the one-sigma confidence interval for the theoretical regression curve is reported to be <1% for $E/\lambda U$ values 0.034 to 0.92 and <5% at the end points. For the L cross sections the figures reported are <2% for $E/\lambda U$ values 0.084 to 2.33 and <8% to the end points.

Table 6
COEFFICIENTS FOR THE CALCULATION OF X-RAY IONIZATION CROSS SECTIONS USING EQUATION 19

Coefficients	K X-rays	L X-rays
b_0	2.0471	3.6082
b_1	−0.65906 (−2)	0.37123
b_2	−0.47448	−0.36971
b_3	0.99190 (−1)	−0.78593 (−4)
b_4	0.46063 (−1)	0.25063 (−2)
b_5	0.60853 (−2)	0.12613 (−2)

From Johansson, S. A. E. and Johansson, T. B., *Nucl. Instrum. Methods*, 137, 473 (1976). (With permission.)

5. Theoretical Values for Cross Sections

As an alternative to the above approach one can employ the cross-section values obtained from the various theoretical predictions previously discussed. For convenience in computer calculations, Reuter et al.[17] have fitted a 7th order polynomial to the tabulation of Garcia et al.[49] for the universal function of the BEA theory. The K shell ionization cross section is obtained from the polynomial

$$\log_{10}(U^2 \sigma_1/Z^2) = \sum_{n=0}^{7} (\log_{10} E/\lambda U)^n A_n \qquad (20)$$

where the coefficients are given in Table 7, and U is in keV. This log-log power series fit reproduces the tabulated data to better than 1%. It should be noted, however, as pointed out by Johansson and Johansson,[31] that the agreement between theory and experiment is rather poor in the region of interest.

VI. THICK SAMPLES

It is often found that samples requiring analysis have a thickness which is greater than the range of the incident protons in the sample. In addition, it is often essential that the integrity of these samples is retained. Under these circumstances the sample is analyzed in its natural state and is defined as a thick sample. A less rigorous definition is often employed; in general, a thick sample is regarded as one in which occurs significant attenuation of the incident protons and absorption of the emitted X-rays in the sample. To establish the thickness of a sample with respect to the incident protons the range of the protons in that sample must be obtained from range data tabulations. Since the range of the proton depends on its initial energy the thickness of a sample is energy dependent. For example, a 25-μm silicon sample will be infinitely thick with respect to a 1-MeV proton beam but not to a 2-MeV proton beam.

The analysis of thick samples tends to be more complicated than the analysis of thin samples for three main reasons:

1. The X-ray production cross section does not remain constant in a thick target, as it is energy dependent, and the proton energy varies from its maximum, incident energy, right down to zero when it is brought to rest in the sample.

Table 7
COEFFICIENTS FOR THE CALCULATION OF K-SHELL IONIZATION CROSS SECTIONS USING EQUATION 20

Coefficients	K X-rays
A_0	−19.04
A_1	0.03028
A_2	−1.11
A_3	0.3771
A_4	0.1923
A_5	−0.07459
A_6	−0.05084
A_7	−0.005949

2. The X-rays produced within the sample are produced at different depths and hence the absorption of the X-rays in emerging from the sample varies.
3. The X-rays produced by the main body of the sample, the matrix, may produce the X-rays of interest by secondary fluorescence of the atoms.

In addition, as discussed by Willis et al.,[98] thick sample analyses have been criticized because any inhomogeneities within the sample, coupled with the small quantity of the material sampled by the proton beam, means that the analysis may not be representative of the bulk sample. These are precisely the conditions required, however, if spatial information is required and represents one of the important characteristics of PIXE analysis. If information on the average content of the sample is required this can only be approached by allowing the beam to sample as large an area as possible. Alternatively, if the sample integrity is not important, certain samples can be ground, and then pressed into a pellet using a suitable high pressure press. A schematic diagram for the analysis of a thick sample is shown in Figure 26.

A. Thick Sample Formulation

To establish the equations for a thick sample we assume that a thick homogeneous sample containing N atoms per unit volume of the element of interest is bombarded with n_o protons of energy E_p. If we assume that there is no production of X-rays of interest by the matrix X-rays, then the X-ray yield is obtained by integrating the yield from an elementary thickness dx of the sample over the range of the proton. The yield is then given by

$$Y = n_o N \int_0^{\text{Range}} \sigma_x \, dx \qquad (21)$$

It is often more convenient to express this integral in terms of the energy rather than the thickness. To do this we note that $\frac{dY}{dE} = \frac{dY}{dx}\frac{dx}{dE}$ and that when x = o, i.e., the surface of the sample, the proton energy is E_p, and when x = range of the proton, the proton energy is zero. Hence Equation 21 becomes

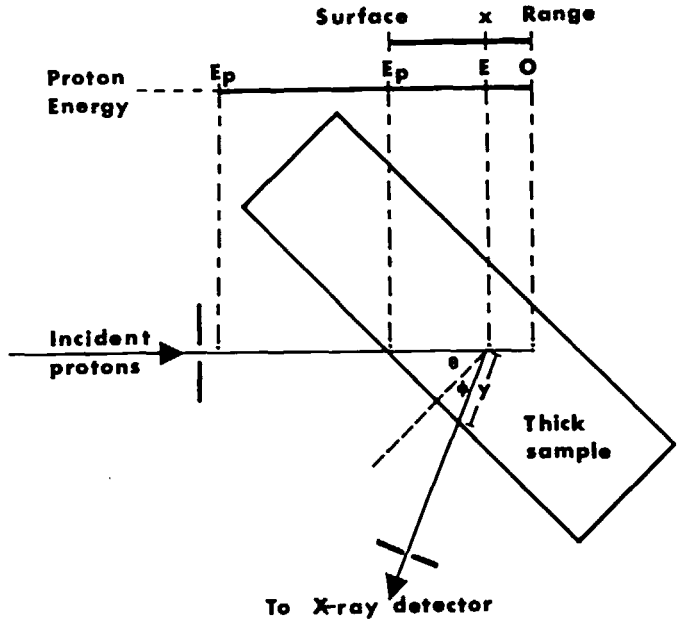

FIGURE 26. Schematic of a thick sample showing the incident proton beam and emerging X-rays.

$$Y = n_o N \int_{E_p}^{o} \sigma_x \, (dE/dx)^{-1} \, dE \tag{22}$$

where (dE/dx) is the stopping power of the matrix. Since the energy of the protons decreases as they penetrate the sample, Equation 22 is more conveniently expressed as follows:

$$Y = n_o N \int_{o}^{E_p} \sigma_x \, (-dE/dx)^{-1} \, dE \tag{23}$$

The area $A_{\alpha i}$ (E) under the K_α X-ray peak corresponding to the i^{th} element in the resulting X-ray spectrum is given by

$$A_{\alpha i}(E) = N_i \, n_o \, \epsilon_{\alpha i} \frac{d\Omega}{4\pi} e^{-\sum \mu_j S_j} \int_{o}^{E_p} \sigma_{\alpha i}(E) \, (-dE/dx)^{-1} \, e^{-\mu_i y} \, dE \tag{24}$$

where N_i is the number of atoms per unit volume of the i^{th} element, $\sigma_{\alpha i}$ is the K_α production cross section for the i^{th} element, $\epsilon_{\alpha i}$ is the efficiency of the detector for the K_α radiation of the i^{th} element, $d\Omega$ is the detector solid angle, $e^{-\mu_j S_j}$ is the attentuation of the K_α X-rays of the i^{th} element in the j^{th} absorber of thickness S_j, between the target and detector, $e^{-\mu_i y}$ is the absorption of the K_α X-ray of the i^{th} matrix element in the matrix in emerging along a path of length y.

The path y along which the X-rays emerge before detection clearly depends on the angle of observation, as shown in Figure 26. If the detector is positioned at an angle of specular reflection of the beam than $\theta = \Phi$ and y, which is given by $y = x\cos\Theta/\cos\Phi$ can be replaced by x, thus simplifying the expression. The quantities $\epsilon_{\alpha i}$, $d\Omega$, and $e^{-\sum_j \mu_{ij} S_j}$ can be determined as described for thin target analysis.

The integral in Equation 24 can be evaluated numerically if $\sigma_{\alpha i}$ (E), (−dE/dx), and μ_{ij} are known. The K_α production cross section is given by

$$\sigma_{\alpha i} = \sigma_{ii}\, R_i\, \omega_i \tag{25}$$

where ω_i = fluorescent yield for the i^{th} element, $R_i = K_\alpha/K_{total}$ intensity ratio for the i^{th} element, and σ_{ii} = ionization cross section for the i^{th} element. The fluorescent yield can be obtained from the tabulation of Bambynek et al.[38] or Krause.[39] Alternatively, for computer use, the following empirical relationship given by Bambynek et al.[38] can be used:

$$\left[\omega_{Ki}/(1-\omega_{Ki})\right]^{1/4} = 0.15 + 0.0327Z_i - 0.64 \times 10^{-6} Z_i^3 \tag{26}$$

where ω_{Ki} is the K X-ray fluorescence yield, and Z_i is the atomic number of the i^{th} element. R_i, the K_α/K intensity ratio, can be found from the theoretical predictions of Scofield,[124] or from experimental measurements of McCrary et al.,[125] Slivinsky and Ebert,[126] Hansen et al.,[127] Richard et al.,[128] Akselsson and Johansson,[129] and Bissinger et al.[130,131] The X-ray production cross sections can be obtained in a similar manner to that previously discussed.

A considerable number of data sets of stopping power of the elements have appeared in the literature. Of the more comprehensive are the tabulations of Williamson et al.,[132] Janni,[133] and Northcliffe and Schilling.[134] The tabulation of Williamson et al.[132] provides energy loss and range data for 37 elements with atomic numbers in the range Z = 1 to Z = 92 for protons, deuterons, helium 3 ions, and alpha particles. The tabulation covers the energy range of 0.05 MeV to 100 MeV and is based on an empirical modification of the Bethe formulation.

A comprehensive tabulation of 103 projectile ion types has been presented by Northcliffe and Schilling[134] in the energy region of 0.0125 to 12 MeV/u. The data set covers 24 elements and was derived from experimental data for ions on aluminium using appropriate theoretical and empirical formulations. The extensive tabulation of Janni[133] gives the proton energy loss, path length, range, multiple scattering, and straggling for 74 elements. The energy range covered is from 0.1 to 1000 MeV. Between 0.1 MeV and 1 MeV the values of energy loss were obtained by smoothing and interpolating experimental data. Above 1 MeV, the Bethe formulation was employed.

A computer program has been developed by Steward[135] for calculating stopping power and range data for heavy ions of energy 0.01 to 500 MeV/u for any nongaseous element. For incident ions with atomic number $\leqslant 10$ and energies below 10 MeV/u the program is based on experimental data. A very comprehensive method of calculating stopping power and range data has been reported by Armstrong and Chandler.[136] Their program, SPAR, is designed to calculate stopping power and ranges for heavy ions in any nongaseous medium for energies ranging from zero to several hundred GeV. The SPAR code is the only general source of low energy data available.

Andersen[137] has presented a detailed bibliography and index of experimental stopping power and range data and this has been employed by Anderson and Ziegler[138] to obtain semiempirical stopping power and ranges for protons in all elements. Only absolute experimental data were considered, to which an analytical function was fitted using

iterative computer techniques. For the elements for which no experimental data exist the authors have extended their fitting parameters by interpolation. The range of proton energies covered is 10 keV $<$ E/u $<$ 20 MeV. Above 2 MeV the agreement with experimental data is of the order of 1%, at lower energies considerably more scatter is noticeable. Clearly, for a given element, reference to all available data is the safest course of action.

When the sample matrix contains more than one atomic component contributing to the stopping power, the total stopping power is the weighted addition of the individual components, Bragg-Kleeman's rule,

$$S_m(E) = \sum_{1}^{n} C_i S_i(E) \qquad (27)$$

where $S_m(E)$ is the stopping power of the matrix for projectile energy E, n is the number of atomic components, $S_i(E)$ is the stopping power of the i^{th} component, and C_i is the fraction of the i^{th} component in the matrix.

Bewers and Flack[139] have investigated the stopping power of 16 different fluorine compounds for 1 MeV protons and found that the deviation from Bragg's rule was less than 2%. Feng et al.[140] studied the applicability of the additive rule in binary metal alloys and metal oxides using MeV $^4He^+$ ions. They found no deviations from the rule for Au-Ag, Au-Cu, Au-Aℓ, α-Fe_2O_3 and Fe_3O_4, but obtained a 20% discrepancy in $Aℓ_2O_3$. A study by Powers et al.[141] and a survey by Ziegler et al.[142] for MeV alphas suggests that departures from additivity up to 20% are to be expected between solid and gaseous forms of an element, such as oxygen, due to molecular effects. More recently, Blondiaux et al.,[143] using the average stopping power method discussed by Ishii et al.,[144] experimentally determined the stopping power ratio of five metals and their associated oxides using protons and compared the results with the calculated ratios using the data of Anderson and Ziegler[138] for the stopping power of the metals and gaseous oxygen. The agreement obtained was better than 1.1%. The authors conclude that above the energies considered (average energy $E_m > 2.35$ MeV/u and threshold > 1 MeV/u) deviations from the additive rule for the oxides investigated are negligible and that the data of Anderson and Ziegler[138] for hydrogen can be used with confidence.

In a similar way the effective absorption coefficient for the matrix for a particular X-radiation can be obtained. Hence, if μ_i is the effective absorption coefficient of the matrix to K_α radiation from the i^{th} element, then

$$\mu_i = \sum_{1}^{n} C_{ij} \mu_{ij} \qquad (28)$$

where μ_{ij} is the mass absorption coefficient of the j^{th} element in the matrix for the K_α radiation of the i^{th} element, and C_{ij} is the fraction of the j^{th} element present in the matrix.

Once the integral of Equation 24 is evaluated it remains only to irradiate the sample with protons of energy E and determine the area $A_{\alpha_i}(E)$ under the K_α X-ray peak corresponding to the i^{th} element in the spectrum for n_o protons incident on the sample. Equation 24 can then be evaluated and the concentration N_i of element i in the sample determined. Since the X-ray production cross section decreases rapidly with decreasing energy the major part of the X-ray yield is produced in the surface of the sample in which the protons lose 30% of their energy. As pointed out by Deconninck et al.[30] a good approximation to the integral in Equation 24 can be obtained by changing the lower limit of the integral from 0 to 0.7E, thus reducing the computational procedure considerably.

B. Use of Standards

A common practice for thick target measurements is the use of a standard material of similar composition containing a known amount of the element of interest. The sample and the standard material are bombarded sequentially with protons of a fixed energy and the X-ray yield determined for a fixed number of protons. The advantage of the method lies in the fact that many of the parameters, such as detector efficiency, ϵ, and solid angle, $d\Omega$, that appear in Equation 24 for the yield are eliminated. If the sample and standard are homogeneous, and contain N_i and N_s atoms per unit volume, respectively, of the element of interest, then for a fixed proton energy E_p

$$\frac{A_{\alpha i}}{A_{\alpha s}} = \frac{N_i}{N_s} \frac{\int_{0.7E_p}^{E_p} (\sigma_{\alpha i}(E)/S(E))\, e^{-\mu i x}\, dE}{\int_{0.7E_p}^{E_p} (\sigma_{\alpha i}(E)/S_s(E))\, e^{-\mu i x_s}\, dE} \tag{29}$$

where $S(E)$ and $S_s(E)$ are the stopping powers of the sample and standard, respectively, and $e^{-\mu i x}$ and $e^{-\mu i x_s}$ are the absorption corrections for the sample and standard. The integrals are evaluated as discussed earlier, taking due account of the particular geometry employed. Examples of the absorption for a range of elements in a pure Z matrix, Cu, Fe, and Si matrices and for a cellulose matrix are given by Deconninck et al.[30]

If the element of interest is of high Z material in a low Z matrix then the absorption in the matrix is negligible and the equation reduces to

$$\frac{A_{\alpha i}}{A_{\alpha s}} = \frac{N_i}{N_s} \frac{\int_{0.7E_p}^{E_p} (\sigma_{\alpha ix}(E)/S(E))\, dE}{\int_{0.7E_p}^{E_p} (\sigma_{\alpha ix}(E)/S_s(E))\, dE} \tag{30}$$

from which N_i can be readily obtained.

In the rather special case of the determination of trace elements in homogeneous powders or liquids a reference element can be introduced directly into the sample and employed as an internal standard. A known quantity of the selected element is introduced into the sample and its X-ray yield determined. The concentration of the X-ray yields from the trace elements can then be obtained by comparison with the yield from the standard. It should be stressed, however, that the addition of the standard must not change the X-ray absorption or the (dE/dx) characteristics of the matrix to any great extent if meaningful results are to be obtained.

C. Matrix Effects

So far in the discussion of thick targets we have negelected the enhancement in the X-ray yield due to matrix effects. This enhancement arises from secondary X-ray production of the X-radiation of interest produced by one or more of the following: (a) secondary electrons, (b) bremsstrahlung from protons, (c) bremsstrahlung from

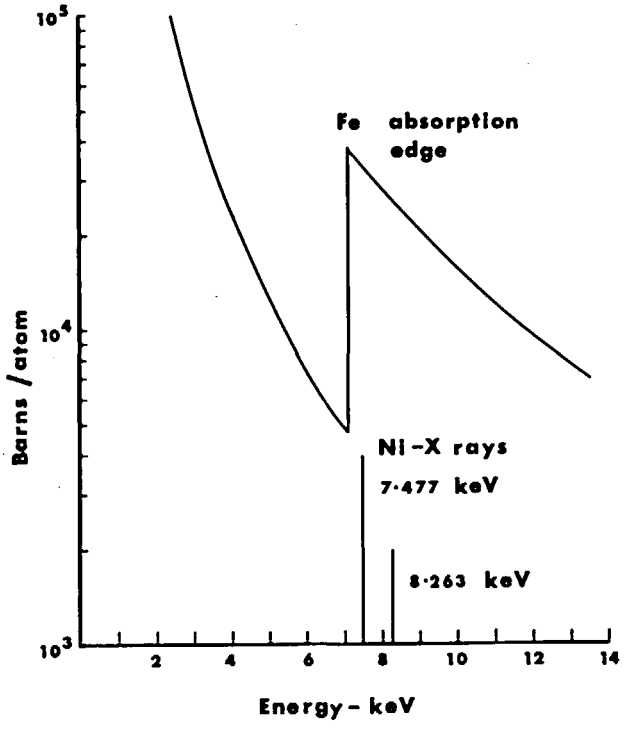

FIGURE 27. Photon absorption cross section for iron as a function of photon energy, showing the iron absorption edge in relation to Ni X-rays.

electrons, (d) target collisions, (e) Auger electrons, and (f) primary induced X-rays. Ahlberg[18] discusses the contribution the above processes make to the total enhancement and concludes that the only source of importance for secondary excitation is primary induced X-rays.

The problem of secondary X-ray production of the X-rays of interest becomes significant in cases where the energy of the primary induced matrix X-rays lies just above the absorption edge of the element of interest, as shown in Figure 27. For example, in the case of 2 MeV protons incident on a 99% Ni/1% Fe alloy, the primary induced nickel K_α X-rays have an energy of 7.47 keV, which is slightly larger than the K absorption edge of iron at 7.11 keV. Under these conditions the probability that the nickel X-rays will interact with the 1% iron in the sample and produce iron X-rays is high, and the iron X-rays so produced may account for 54% of the total iron X-ray yield.[17] Conversely, if the energy of the matrix X-ray is significantly higher than the absorption edge of the element of interest, then secondary X-ray production is considerably reduced. For example, in a 99% Ge/1% Fe alloy, secondary X-ray production of Fe X-rays by the 9.88 keV Ge K_α X-rays accounts for only 8% of the Fe X-ray yield. Reuter et al.[17] have calculated the secondary excitation corrections for a series of binary alloys and radiation combinations. The results of their evaluations are reproduced in Table 8. They have presented a detailed formulation for calculating the correction factors which is closely related to that employed in electron microprobe analysis. Experimental data taken for two binary alloys indicated that an accuracy of ±5% can be achieved if the secondary X-ray production correction factor is applied as appropriate and the effect of the composite matrix on the stopping power is included.

Ahlberg[18] has studied the enhancement effect as a function of proton energy and

Table 8
SECONDARY EXCITATION CORRECTIONS FOR A NUMBER OF BINARY ALLOYS AND RADIATION COMBINATIONS

Proton energy (MeV)	Element B (99% wt)	Element A (1% wt)	$\frac{N_{A,SEC}}{N_{A,PR}}$
4	Ni K	Fe K	0.81
2	Ni K	Fe K	0.54
1	Ni K	Fe K	0.38
0.5	Ni K	Fe K	0.31
2	Zn K	Fe K	0.21
2	Ge K	Fe K	0.08
2	P K	Si K	0.21
2	S K	Si K	0.13
2	Ca K	Si K	0.014
2	Au L	Zn K	0.17
2	Au L	Cu K	0.10
2	Au L	Co K	0.040
2	Au L	Mn K	0.014
2	Se K	Au L	0.28
2	Rb K	Au L	0.19
2	Zr K	Au L	0.10
2	Mo K	Au L	0.046

Note: Conditions are selected favoring secondary production of element A. $N_{A,SEC}$ and $N_{A,PR}$ are the number of $K\alpha$ X-rays of element A produced by secondary and primary excitation, respectively.

From Reuter, F. W., Lurio, A., Cardone, A., and Ziegler, Z. F., *J. Appl. Phys.*, 46, 3194 (1975). (With permission.)

sample thickness for an iron matrix. The experimental results for the manganese and chromium content of National Bureau of Standards low-alloy steel, SRM 1261, after correction for enhancement, are in excellent agreement with the accepted values. Van der Kam et al.[22] have developed a computer code to determine enhancement correction factors. They calculated the corrections for 15 to 20 trace elements in matrices of different atomic number ranging from 6 to 50. The samples considered were 10 mg/cm^2 thick and the beam energy employed was 2.5 MeV. The calculations were tested by analyzing blood serum doped with 1 μg of each of 6 elements. Their corrected results are in very good agreement with the known amount of dopant added to the serum. Lin et al.[23] have studied the matrix effects appropriate to liquid samples containing 100 to 200 μg/mℓ of V, Mn, Fe, Co, and As, in the presence of large quantities of copper, up to 100 mg/mℓ, using an external beam configuration. Quantitative results were obtained by the internal standard method. For elements $Z > 20$ they concluded that no corrections were necessary, provided the copper concentration was kept below 5 mg/mℓ. For copper concentrations in excess of this, changes to the matrix result in X-ray yield enhancement of certain elements, which, coupled with changes in the X-ray absorption, must be evaluated to obtain accurate quantitative results. The experimental and theoretical results for the relative sensitivities for V, Mn, Fe, and As, as a function of copper concentration, were found to be in good agreement. The authors make no comment, however, on the rather poor agreement obtained in the case of cobalt, for copper concentrations above 30 mg/mℓ.

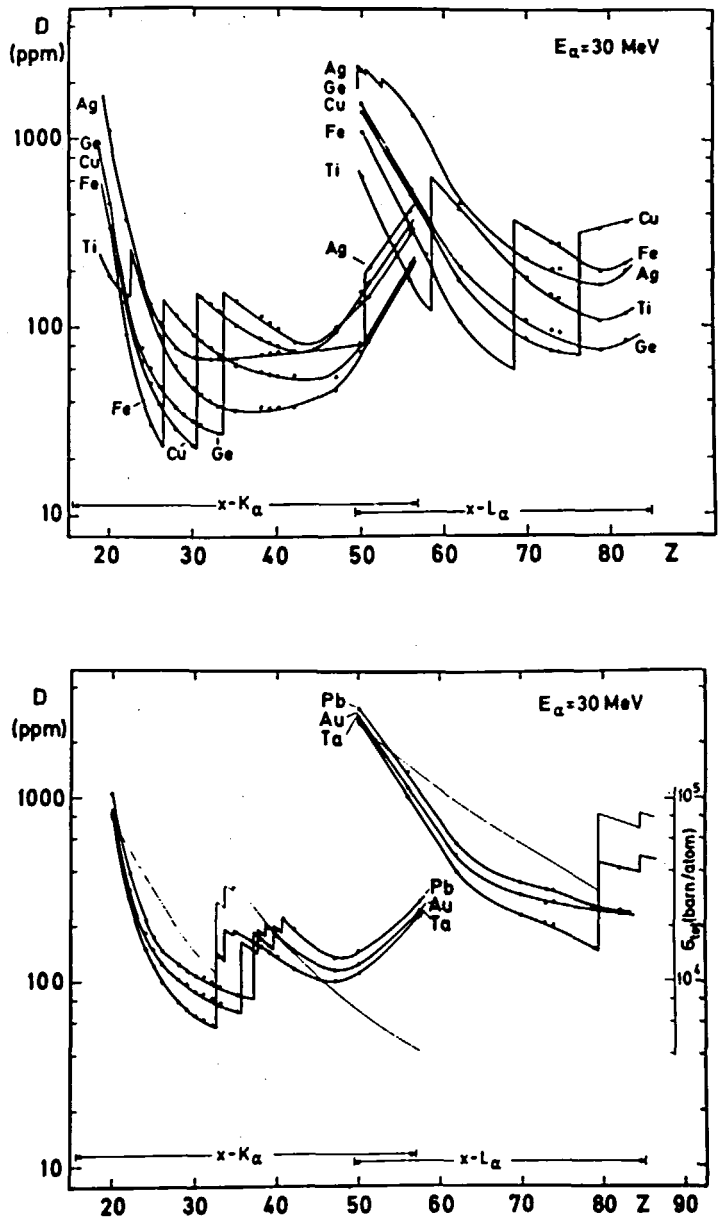

FIGURE 28. Sensitivity of thick samples as a function of atomic number for light and heavy matrices for 1 μC of 30 MeV alphas. (From Hommsen, H., Bauer, K. G., and Fazly, Q., *Nucl. Instrum. Methods*, 157, 305, 1978. With permission.)

D. Sensitivity

The sensitivity achievable in trace analysis of thick samples has been studied by Folkmann,[102] as discussed earlier, and his results for thick and thin samples are reproduced in Figure 21 for carbon and aluminium matrices, giving a range of sensitivities from 10^{-4} to 10^{-9} g/g, depending on Z and the energy employed. The author points out that the calculations are based on the assumption of a homogeneous mixture of elements, and that an inhomogeneous matrix, or surface grains, would produce serious problems with regard to the absorption calculations. Ahlberg et al.[145] report the

sensitivity for 1.0 to 2.5 MeV protons for steel samples to be in the region of 100 ppm, and give the Z dependence of the sensitivity, while Reuter and Lurio[146] obtain sensitivities in NBS low alloy steel standard 461 of the order of 10 ppm with protons of 2.4 MeV energy.

A similar sensitivity of $\leqslant$100 ppm has been reported by Hommsen et al.[147] in their study of PIXE analysis with 30 MeV alpha particles. The Z dependence of the sensitivity is given for a selection of light and heavy matrices, as shown in Figure 28. The discontinuities that occur reflect the absorption edges of the matrix materials. No discontinuity is observed in the sensitivity data presented by Ahlberg et al.,[145] and calculations performed by Hommsen et al.[147] indicate that a discontinuity should be present at the iron absorption edge.

ACKNOWLEDGMENTS

We would like to thank colleagues and staff at the Nuclear Research Centre, Tehran, and the Physics Department of the University of Aston for their continued interest and encouragement in the preparation of this manuscript. In addition, we would like to express our thanks to the support staff, especially the typists, for their invaluable assistance with the manuscript.

REFERENCES

1. **Johansson, T. B., Akselsson, R., and Johansson, S. A. E.,** *Nucl. Instrum. Methods,* 84, 141 (1970).
2. **Johansson, T. B., Akselsson, R., and Johansson, S. A. E.,** *Adv. X-Ray Anal.,* 15, 373, (1972).
3. **Duggan, J. L., Beck, W. L., Albert, L., Munz, L., and Spaulding, J. D.,** *Adv. X-Ray Anal.,* 15, 407, (1972).
4. **Folkmann, F., Borggreen, J., and Kjeldgaard, A.,** *Nucl. Instrum. Methods,* 119, 117 (1974).
5. **Cooper, J. A.,** *Nucl. Instrum. Methods,* 106, 525 (1973).
6. **Perry, S. K. and Brady, F. P.,** *Nucl. Instrum. Methods,* 108, 389 (1973).
7. **Reuter, W. and Lurio, A.,** Detection sensitivities in proton and electron induced X-ray spectroscopy, *Proc. 8th Int. Conf. on X-Ray Optics and Microanalysis,* Boston, 1977.
8. **Ahlberg, M. S. and Adams, F. C.,** *X-Ray Spectrom.,* 7, 73 (1978).
9. **Verba, J. W., Sunier, J. W., Wright, B. T., Slaus, I., Holman, A. B., and Kulleck, J.,** *J. Radioanal. Chem.,* 12, 171 (1972).
10. **Mangelson, N. F., Nielson, K. K., Hill, M. W., Eatough, D. J., and Hansen, L. D.,** *Proc. 3rd Conf. Applications of Small Accelerators,* Denton, Texas, 1974, 163.
11. **Jolly, R. K. and White, H. B.,** *Nucl. Instrum. Methods,* 97, 103 (1971).
12. **Flocchini, R. G., Feeney, P. J., Sommerville, R. J., and Cahill, T. A.,** *Nucl. Instrum. Methods,* 100, 397 (1972).
13. **Walter, R. L., Willis, R. D., Gutknecht, W. F., and Joyce J. M.,** *Anal. Chem.,* 46, 843 (1974).
14. **Valkovic, V.,** *Comtemp. Phys.,* 14, 439 (1973).
15. **Thomas, J. P., Porte, L., Engerran, J., Viala, J. C., and Tousset, J.,** *Nucl. Instrum. Methods,* 117, 579 (1974).
16. **Barns, B. K., Beghian, L. E., Kegel, G. H. R., Mathur, S. C., Mittler A., and Quinn, P. W.,** *Proc. 3rd Conf. on Applications of Small Accelerators,* Denton, Texas, 1974.
17. **Reuter, W., Lurio, A., Cardone, F., and Ziegler, J. F.,** *J. Appl. Phys.,* 46, 3194 (1975).
18. **Ahlberg, M. S.,** *Nucl. Instrum. Methods,* 142, 61 (1977).
19. **Pabst, W.,** *Nucl. Instrum. Methods,* 120, 543, 1974.
20. **Pabst, W.,** *Nucl. Instrum. Methods,* 124, 143, 1975.
21. **Feldman, L. C., Poate, J. M., Ermanis, F., and Schwartz, B.,** *Thin Solid Films,* 19, 81 (1973).
22. **Van der Kam, P. M. A., Vis, R. D., and Verheul, H.,** *Nucl. Instrum. Methods,* 142, 55 (1977).
23. **Lin, T. S., Luo, C. S., and Chou, J. C.,** *Nucl. Instrum. Methods,* 159, 387 (1979).
24. **Huda, W.,** *Nucl. Instrum. Methods,* 158, 587 (1979).
25. Proc. 8th Int. Conf. on X-Ray Optics and Microanalysis, Boston, 1977.
26. 5th Symp. Recent Developments in Activation Analysis, Oxford, England, 1978.
27. 4th Int. Conf. Ion Beam Analysis, Aarhus, Denmark, 1979.
28. Proc. Int. Conf. on Particle Induced X-Ray Emission and its Analytical Applications, *Nucl. Instrum. Methods,* 142, 1977.

29. **Folkmann, F.,** *J. Phys. E,* B11, 429 (1975).
30. **Deconninck, G., Demortier, G., and Bodart, F.,** *At. Energy Rev.,* 13, 367 (1975).
31. **Johansson, S. A. E. and Johansson, T. B.,** *Nucl. Instrum. Methods,* 137, 473 (1976).
32. **Wilk, S. F. J., McKee, J. S. C., and Randell, C. P.,** *Nucl. Instrum. Methods,* 142, 33 (1977).
33. **Van der Heide, J. A., Kivits, H. P. M., and Beuzekam, D. C.,** *X-Ray Spectrom.,* 8, 63 (1979).
34. **Akselsson, K. R. and Johansson, S. A. E.,** *IEEE Trans. Nucl. Sci.,* NS-26, 1358 (1979).
35. **Woldseth, R.,** *X-Ray Energy Spectometry,* Kevex Corp., Burlingame, 1973.
36. **Russ, J. C.,** *Energy Dispersive X-Ray Anlaysis, X-Ray and Electron Probe Analysis,* ASTM Special Technical Publications, 1971, 485.
37. **Storm, E. and Israel, H. I.,** *Nucl. Data Tables,* A7, 565 (1970).
38. **Bambynek, W., Craseman, B., Fink, R. W., Freund, H. V., Mark H., Swift, C. D., Price, R. E. and Rao, P. V.,** *Rev. Mod. Phys.,* 44, 716 (1972).
39. **Krause, M. O.,** *J. Phys. Chem. Ref. Data,* 8, 307 (1979).
40. **Rutledge, C. H. and Watson, R. L.,** *At. Data Nucl. Data Tables,* 12, 195 (1973).
41. **Gardner, R. K. and Gray, T. J.,** *At. Data Nucl. Data Tables,* 21, 515 (1978).
42. **Hardt, T. L. and Watson, R. L.,** *At. Data Nucl. Data Tables,* 17, 107 (1976).
43. **Madison, D. H. and Merzbacher, E.,** *Atomic Inner-Shell Processes.* I, Craseman, B., Ed., Academic Press, New York, 1975.
44. **Taulbjerg, K.,** *Proc. 2nd Int. Conf. on Inner-Shell Ionization,* Mehlhorn, W. and Brenn, R., Eds., Freiburg, West Germany, 1976.
45. **Taulbjerg, K.,** *J. Phys. B,* 10, L341 (1977).
46. **Choi, B. H., Merzbacher, E., and Khandelwal, G. S.,** *At. Data,* 5, 291 (1973).
47. **Basbas, G., Brandt, W., and Laubert, R.,** *Phys. Rev.,* A7, 983 (1973).
48. **Rice, R., Basbas, G., and McDaniel, F. D.,** *At. Data Nucl. Data Tables,* 20, 503 (1977).
49. **Garcia, J. D., Fortner, R. J., and Kavanagh, T. M.,** *Rev. Mod. Phys.,* 45, 111 (1973).
50. **Hansen, J. S.,** *Phys. Rev.,* A8, 822 (1973).
51. **Hansteen, J. M. and Mosebekk, O. P.,** *Nucl. Phys.,* A201, 541 (1973).
52. **Hansteen, J. M., Johnsen, O. M., and Kocbach,L.,** *At. Data Nucl. Data Tables,* 15, 305 (1975).
53. **Khan, M. R., Hopkins, A. G., Crumpton, D., and Francois, P. E.,** *X-Ray Spectrom.,* 6, 140 (1977).
54. **Benka, O. and Kropf, A.,** *At. Data Nucl. Data Tables,* 22, 219 (1978).
55. **Brandt, W. and Lapicki, G.,** *Phys. Rev.,* A20, 465 (1979).
56. **Merzbacher, E. and Lewis, H. W.,** X-ray production by heavy charged particles, in *Encyclopaedia of Physics,* Vol. 34, Flugge, S., Ed., Springer-Verlag, Berlin, 1958, 166.
57. **Akselsson, R. and Johansson, T. B.,** *Nucl. Instrum. Methods,* 91, 663 (1971).
58. **Rickey, F. A., Simms, P. C., and Mueller, K. A.,** *IEEE Trans. Nucl. Sci.,* NS-26, 1347 (1979).
59. **Montenegro, E. C., Baptista, G. B., Leite, C. V. B., De Pinho, A. G., and Paschoa, A. S.,** *Nucl. Instrum. Methods,* 164, 231 (1979).
60. **Bauman, S. E., Williams, E. T., Finston, H. L., Bond, A. H., and Lesser, P. M. S.,** *Nucl. Instrum. Methods,* 165, 57 (1979).
61. **Papper, C. S., Chaudhri, M. A., and Rouse, J. L.,** *Nucl. Instrum. Methods,* 154, 219 (1978).
62. **Feld, E. J. and Umbarger, C. J.,** *Nucl. Instrum. Methods,* 103, 341 (1972).
63. **Valkovic, V., Liebert, R. B., Zabel, T., Larson, H. T., Miljanic, D., Wheeler, R. M., and Phillips, G. C.,** *Nucl. Instrum. Methods,* 114, 573 (1974).
64. **Orsini, C. Q. and Boueres, L. C.,** *Nucl. Instrum. Methods,* 142, 27 (1977).
65. **Lecomte, R., Paradis, P., Monaro, S., Barrette, M., Lamoureux, G., and Ménard, H. A.,** *Nucl. Instrum. Methods,* 150, 289 (1978).
66. **Jolly, R. K., Kane, J. R., Buckle, D. C., Randers-Pehrson, G., Teoh, W., and Aceto, H.,** *Nucl. Instrum. Methods,* 151, 183 (1978).
67. **Raith, B., Roth, M., Göllner, K., Gonsior, B., Ostermann, H., and Uhlhorn, C. D.,** *Nucl. Instrum. Methods,* 142, 39 (1977).
68. **Hansen, J. S., McGeorge, J. C., Nix, D., Schmidt-Ott, W. D., Unus, I., and Fink, R. W.,** *Nucl. Instrum. Methods,* 106, 365 (1973).
69. **Wood, R. E., Roa, P. V., Puckett, O. H., and Palms, J. M.,** *Nucl. Instrum. Methods,* 94, 245 (1971).
70. **Gehrke, R. J. and Lokken, R. A.,** *Nucl. Instrum. Methods,* 97, 219 (1971).
71. **Gallagher, W. J. and Cipolla, S. J.,** *Nucl. Instrum. Methods,* 122, 405 (1974).
72. **Campbell, J. L. and McNelles, L. A.,** *Nucl. Instrum. Methods,* 101, 153 (1972).
73. **Campbell, J. L., O'Brian, P. O., and McNelles, L. A.,** *Nucl. Instrum. Methods,* 92, 269 (1971).
74. **Johnson, G. A., Manson, E. L., and O'Foghludha, F.,** *Nucl. Instrum. Methods,* 151, 217 (1978).
75. **Shima, K.,** *Nucl. Instrum. Methods,* 165, 21 (1979).
76. **Gedcke, D. A.,** *X-Ray Spectrom.,* 1, 129 (1972).
77. **Reed, S. J. B.,** *J. Phys. E,* 5, 994 (1972).

78. Khan, M. R. and Crumpton, D., *Nucl. Instrum. Methods,* 144, 351 (1977).
79. Jaklevic, J. M., Goulding, F. S., and Landis, D. A., *IEEE Trans. Nucl. Sci.,* NS-19, 392 (1972).
80. Cahill, T. A., Ion-excited X-ray analysis of environmental samples, in *New Uses of Ion Accelerators,* Ziegler, J. F., Ed., Plenum Press, New York, 1975, 1.
81. Koenig, W., Richter, F. W., Steiner, U., Stock, R., Thielmann, R., and Wätjen, U., *Nucl. Instrum. Methods,* 142, 225 (1977).
82. Mingay, D. W., Jonker, W. D., and Smith, B. J., *At. Energy Board, Repub. S. Afr.,* [*Rep.*] PEL-259, 1978.
83. Choy, S. C. and Schmitt, R. A., *Nature (London),* 205, 758 (1965).
84. Routtie, J. T. and Prussin, S. G., *Nucl. Instrum. Methods,* 72, 125 (1969).
85. Mariscotti, M. A., *Nucl. Instrum. Methods,* 50, 309 (1967).
86. Johansson, T. B., Van Grieken, R. E., Nelson, J. W., and Winchester, J. W., *Anal. Chem.,* 47, 855 (1975).
87. Schnick, W. C., Ames Laboratory, USERDA, University of Iowa, Iowa City, IS-3460, 1974, and IS-3636, 1975.
88. Lien, Y. C., Zombola, R. R., and Bearse, R. C., *Nucl. Instrum. Methods* 146, 609 (1977).
89. Willis, R. D. and Walter, R. L., *Nucl. Instrum. Methods,* 142, 231 (1977).
90. Bevington, P. R., *Data Reductions and Error Analysis for Physical Sciences,* McGraw-Hill, New York, 1969, 235.
91. Hasselmann, I., Kroenig, W., Richter, F. W., Steiner, U., Bode, J. C., and Ohta, W., *Nucl. Instrum. Methods,* 142, 163 (1977).
92. Van Espen, P., Nullens, H., and Adams, F., *Nucl. Instrum. Methods,* 142, 243 (1977).
93. Kaufmann, H. C. and Akselsson, K. R., *Adv. X-Ray Anal.,* 18, 353, (1975).
94. Kaufmann, H. C., Akselsson, K. R., and Courtney, W. J., *Nucl. Instrum. Methods,* 142, 251 (1977).
95. Kaufmann, H. C., Akselsson, K. R., and Courtney, W. J., *Adv. X-Ray Anal.,* 19, 355 (1976).
96. Nass, M. J., Lurio, A., and Ziegler, J. F., *Nucl. Instrum. Methods,* 154, 567 (1978).
97. Yule, H. P., *Anal. Chem.,* 38, 103 (1966).
98. Willis, R. D., Walter, R. L., Shaw, R. W., and Gutknecht, W. F., *Nucl. Instrum. Methods,* 142, 67 (1977).
99. Folkmann, F., Gaarde, C., Huus, T., and Kemp., K., *Nucl. Instrum. Methods,* 116, 487 (1974).
100. Ishii, K., Kamiya, M., Sera, K., Morita, S., and Tawara, H., *Phys. Rev.,* A15, 2126 (1977).
101. Campbell, J. L., *Nucl. Instrum. Methods,* 142, 263 (1977).
102. Folkmann, F., Sensitivity in trace element analysis of thick samples using proton induced X-rays, in *Ion Beam Surface Layer Analysis, 2,* Meyer, O., Linker, G., and Käppeler, F., Eds., Plenum Press, New York, 1976, 747.
103. Camp, D. C., Cooper, J. A., and Rhodes, J. R., *X-Ray Spectrom.,* 3, 47 (1974).
104. Baum, R. M., Willis, R. D., Walter, R. L., Gutknecht, W. F., and Stiles, A. R., *X-ray Fluorescence Analysis of Environmental Samples,* Dzubay, T. G., Ed., Ann Arbor Sci., Ann Arbor, Mich., 1977, 165.
105. Kivits, H. P. M., De Rooij, F. A. J., and Wijnhoven, G. P. J., *Nucl. Instrum. Methods,* 164, 225 (1979).
106. Kemp, K., Jenson, F. P., Moller, J. T., and Gyrd-Hansen, N., *Phys. Med. Biol.* 20, 834, (1975).
107. Campbell, J. L., Orr, B. H., Herman, A. W., McNelles, L. A., Thomson, J. A., and Cook, W. B., *Anal. Chem.,* 47, 1542 (1975).
108. Jolly, R. K., Pehrson, G. R., Gupta, S. K., Buckle, D. C., and Aceto, H., *Proc. 3rd Conf. on Applications of Small Accelerators,* Denton, Texas, 1974.
109. Valkovic, V., Rendic, D., and Phillips, G. C., *Environ. Sci. Technol.,* 9, 1150 (1975).
110. Rudolph, H., Kliwer, J. K., Kraushaar, J. J., Ristinen, R. A., and Smythe, W. R., *18th Annu. Symp. Anal. Instrum.,* 10, 151 (1972).
111. Bearse, R. C., Close, D. A., Malanify, J. J., and Umbarger, C. J., *Anal. Chem.,* 46, 499 (1974).
112. Mangelson, N. F., Hill, M. W., Nielson, K. K., and Ryder, J. F., *Nucl. Instrum. Methods,* 142, 133 (1977).
113. Gorsuch, T. T., *The Destruction of Organic Matter,* Pergamon Press, Oxford, 1970.
114. Walter, R. L., Willis, R. D., Gutknecht, W. F., and Shaw, R. W., *Nucl. Instrum. Methods,* 142, 181 (1977).
115. Nielson, K. K., thesis, Brigham Young Univ., Provo, Utah, 1975.
116. Rickey, F. A., Mueller, K. A., Simms, P. C., and Michael, B. D., Sample preparation for multielemental analysis of water, in *X-Ray Fluorescence Analysis of Environmental Samples,* Dzubay, T. G., Ed., Ann Arbor Sci., Ann Arbor, Mich., 1977, 134.
117. Lochmüller, C. H., Galbraith, J. W., and Walter, R. L., *Anal. Chem.,* 46, 440 (1974).
118. La Fleur, P. D., *J. Radioanal. Chem.,* 19, 227 (1974).

119. **Bowen, H. J. M.,** *J. Radioanal. Chem.,* 19, 215 (1974).
120. **Simms, P. C. and Rickey, F. A.,** The Multielemental Analysis of Drinking Water Using Proton-Induced X-Ray Emission (PIXE), U. S. Environmental Protection Agency Report EPA-600/1-78-058, Purdue University, West Lafayette, Ind., 1978.
121. **Akselsson, K. R., Johansson, S. A. E., and Johansson, T. B.,** *X-Ray Fluorescence Analysis of Environmental Samples,* Dzubay, T. G., Ed., Ann Arbor Sci., Ann Arbor, Mich., 1977, 175.
122. **Millar, R. H. and Greening, J. R.,** *J. Phys. B,* 7, 2332 (1974).
123. **Khan, M. R., Hopkins, A. G., and Crumpton, D.,** *Proc. 8th Int. Conf. on X-ray Optics and Microanalysis,* Boston, 1977.
124. **Scofield, J. H.,** *Phys. Rev.,* 179, 9 (1969).
125. **McCrary, J. H., Singman, L. V., Ziegler, L. H., Looney, L. D., Edmunds, C. M., and Harris, C. E.,** *Phys. Rev.,* A5, 1587 (1972).
126. **Slivinsky, V. W. and ebert, P. J.,** *Phys. Rev.,* A5, 1581 (1972).
127. **Hansen, J. S., Freund, H. W., and Fink, R. W.,** *Nucl. Phys.,* A142, 604 (1970).
128. **Richard, P., Bonner, T. I., Furuta, T., Morgan, I. L., and Rhods, J. R.,** *Phys. Rev.,* A1, 1044 (1970).
129. **Akselsson, R. and Johansson, T. B.,** *Z. Phys.,* 266, 245 (1974).
130. **Bissinger, G. A., Shafroth, S. M., and Waltner, A. W.,** *Phys. Rev.,* A5, 2046 (1972).
131. **Bissinger, G. A., Basksin, A. B., Choi, B. H., Shafroth, S. M., Howard, J. M., and Waltner, A. W.,** *Phys. Rev.,* A6, 545 (1972).
132. **Williamson, C. F., Boujot, J. P., and Picard, J.,** Tables of Range and Stopping Power of Chemical Elements for Charged Particles of Energy 0.05 to 500 MeV, Report No. CEA-R 3042, C. E. A., Saclay, France, 1967.
133. **Janni, J. F.,** Calculation of energy loss, range, path length, straggling, multiple scattering and the probability of inelastic nuclear collisions from 0.1 to 1000 MeV protons, *Technical Report AFWL-TR-65-150,* Air Force Weapons Laboratory, 1966.
134. **Northcliffe, L. C. and Schilling, R. F.,** *Nucl. Data Tables,* A7, 233 (1970).
135. **Steward, P. G.,** thesis, University of California, Berkeley, 1968.
136. **Armstrong, T. W. and Chandler, K. C.,** SPAR, a fortran program for computing stopping powers and ranges for muons, charged pions, protons, and heavy ions, *Report ORNL-4869,* Oak Ridge National Laboratory, 1973.
137. **Anderson, H. H.,** Bibliography and index of experimental range and stopping power, in *The Stopping Power and Ranges of Ions in Matter, 2, Pergamon Press, New York, 1977.*
138. **Andersen, H. H. and Ziegler, J. F.,** Hydrogen-stopping powers and ranges in all elements, in *The Stopping Power and Ranges of Ions in Matter, 3,* Pergamon Press, New York, 1977.
139. **Bewers, J. M. and Flack, F. C.,** *Nucl. Instrum. Methods,* 59, 337 (1968).
140. **Feng, J. S. Y., Chu, W. K., and Nicolet, M. A.,** *Thin Solid Films,* 19, 227 (1973).
141. **Powers, D., Lodhi, A. S., Lin, W. K., and Cox, H. L.,** *Thin Solid Films,* 19, 205 (1973).
142. **Ziegler, J. F., Chu, W. K., and Feng, J. S. Y.,** *App. Phys. Lett.,* 27, 387 (1975).
143. **Blondiaux, G., Valladon, M., Ishii, K., and Debrun, J. L.,** *Trans. Am. Nucl. Soc.,* 32, 199 (1979).
144. **Ishii, K., Valladon, M., and Debrun, J. L.,** *Nucl. Instrum. Methods,* 150, 213 (1978).
145. **Ahlberg, M., Akselsson, R., Brune, D., and Lorenzen, J.,** *Nucl. Instrum. Methods,* 123, 385 (1975).
146. **Reuter, W. and Lurio, A.,** Detection sensitivities for thick specimens in proton and electron induced X-ray spectrometry, in *IBM Research Report,* T. J. Watson Research Centre, Yorktown Heights, New York, 1977.
147. **Hommsen, H., Bauer, K. G., and Fazly, Q.,** *Nucl. Instrum. Methods,* 157, 305 (1978).
148. **Alder, K., Huus, T., Mottelson, B., and Winter, A.,** *Rev. Mod. Phys.,* 28, 432 (1956).
149. **Mingay, D. W. and Barnard, E.,** *Nucl. Instrum. Methods,* 157, 537 (1978).
150. **Willis, R. D., Walter, R. L., Doyle, B. L., and Shafroth, S. M.,** *Nucl. Instrum. Methods,* 142, 317 (1977).
151. **Watson, R. L., Leeper, A. K., and Sonobe, B. I.,** *Nucl. Instrum. Methods,* 142, 311 (1977).
152. **McGuire, E. J.,** *Phys. Rev.,* A3, 587 (1971).
153. **Khan, M. R.,** Ph.D. thesis, University of Aston, Birmingham, England, 1976.
154. **Tawara, H., Ishii, K., Morita, S., Kaji, H., and Shiokawa, T.,** *Phys. Rev.,* All, 1560 (1975).
155. **Close, D. A., Bearse, R. C., Malanify, J. J., and Umbarger, C. J.,** *Phys. Rev.,* A8, 1873 (1973).
156. **Shabason, L., Cohen, B. L., Wedberg, G. H., and Chan, K. K.,** *J. Appl. Phys.,* 44, 4749 (1973).
157. **Abrath, F. and Gray, T. J.,** *Phys. Rev.,* A9, 682 (1974).
158. **Musket, R. G. and Bauer, W.,** *J. Appl. Phys.,* 43, 4786 (1972).
159. **Gordon, B. M. and Kraner, H. W.,** *J. Radioanal. Chem.,* 12, 181 (1972).
160. **Herman, A. W., McNelles, L. A., and Campbell, J. W.,** *Nucl. Instrum. Methods,* 109, 429 (1973).
161. **Chemin, J. E., Mitchell, I. V., and Saris, F. W.,** *J. Appl. Phys.,* 45, 532 (1974).
162. **Gray, T. J., Lear, R., Dexter, R. J., Schwettmann, F. N., and Wiemer, K. C.,** *Thin Solid Films,* 19, 103 (1973).

163. Cairns, J. A., *Surface Sci.,* 34, 638 (1973).
164. Cairns, J. A., Marwick, A. D., and Mitchell, I. V., *Thin Solid Films,* 19, 91 (1973).
165. Pabst, W. and Schmid, K., *X-Ray Spectrom.,* 85, 4 (1975).
166. Garten, R. P. H., Groeneveld, K. O., Köenig, K. H., and Schader, J., *IEEE Trans. Nucl. Sci.,* NS-26, 1381 (1979).
167. Garten, R. P. H., Groeneveld, K. O., and Köenig, K. H., *Z. Anal. Chem., 288, 171 (1977).*
168. Shroy, R. E., Soo, P., Sastre, C. A., Schweitzer, D. G., Kraner, H. W., and Jones, K. W., *IEEE Trans. Nucl. Sci.,* NS-26, 1386 (1979).
169. Van Grieken, R. E., Johansson, T. B., Winchester, J. W., and Odom, L. A., *Z. Anal. Chem.,* 275, 343 (1975).
170. Annegarn, H. J., Keddy, R. J., Madiba, C. C. P., Renan, M. J., and Sellschop, J. P. F., *Adv. X-Ray Anal.,* 21, 245 (1977).
171. Kirchner, S. J., Oona, H., Fernando, Q., Lee, J. H., and Zeitlin, H. Z., *Anal. Chem.,* 50, 1701 (1978).
172. Ahlberg, M., Akselsson, R., Forkman, B., and Rausing, G., *Archaeometry,* 18, 39 (1976).
173. Baijot-Stroobants, J. and Bodart, F., *Nucl. Instrum. Methods,* 142, 293 (1977).
174. Peisach, M., Meyer, B. R., and Van Heerden, I. J., *Particle Induced X-Ray Spectrometry,* South Universities Nuclear Institute, SUNI 39, South Africa, 1975.
175. Sioshansi, P., Lodhi, A. S., and Payrovan, H., *Nucl. Instrum. Methods,* 142, 285 (1977).
176. Deconninck, G., *Nucl. Instrum. Methods,* 142, 275 (1977).
177. Campbell, J. L, Orr, B. H., and Noble, A. C., *Nucl. Instrum. Methods,* 142, 289 (1977).
178. Bearse, R. C., Burns, C. E., Close, D. A., and Malanify, J. J., *Nucl. Instrum. Methods,* 142, 289 (1977).
179. Boro, R. T. and Cipolla, S. J., *Nucl. Instrum. Methods,* 131, 343 (1975).
180. Vis, R. D., Van der Kam, P. M. A., and Verheul, H., *Nucl. Instrum. Methods,* 142, 159 (1977).
181. Valkovic, V., *Nucl. Instrum. Methods,* 142, 151 (1977).
182. Barrette, M., Lamoureux, G., Lebel, E., Lecomte, R., Paradis, P., and Monaro, S., *Nucl. Instrum. Methods,* 134, 189 (1976).
183. Hrgovcic, M., Tessmer, C. F., Thomas, F. B., Fuller, L. M., Gamble, J. F., and Shüllenberger, C. C., *Cancer,* 31, 1337 (1973).
184. Tessmer, C. F., Hrgovcic, M., Thomas, F. B., Fuller, L. M., and Castro, J. R., *Radiology,* 106, 635 (1973).
185. Altman, P. L. and Dittmer, D. S., *Biology Data Book,* Vol. 3, Fed. Am. Soc. Exp. Biol., Bethesda, Md., 1976.
186. Simpson, A. E. and Dyson, N. A., *Nucl. Instrum. Methods,* 146, 473 (1977).
187. Dabek, J. T., Dyson, N. A., and Simpson, A. E., Quantitative applications of proton-induced X-ray emission analysis in the fields of medicine and biology, in *Proc. 8th Int. Conf. on X-Ray Optics and Microanalysis,* Boston, 1977.
188. Van Rinsvelt, H. A., Lear, R. D., and Adams, W. R., *Nucl. Instrum. Methods,* 142, 171 (1977).
189. Mangelson, N. F., Hill, M. W., Nielson, K. K., Eatough, D. J., Christensen, J. J., Izatt, R. M., and Richards, D. O., *Anal. Chem.,* 51, 1187 (1979).
190. Cookson, J. A. and Pilling, F. D., *Phys. Med. Biol.,* 20, 1015 (1975).
191. Grodzins, L., Horowitz, P., and Ryan, J., The scanning proton microprobe in an atmospheric environment, *4th Int. Conf. on Scientific and Industrial Applications of Small Accelerators,* Duggan, J. L. and Morgan, I. L., Eds., IEEE, New York, 1976, 75.
192. Campbell, J. L., *IEEE Trans. Nucl. Sci.,* NS26, 1363 (1979).
193. Nelson, J. W., Winchester, J. W., and Akselsson, R., *Proc. 3rd Conf. on Applications of Small Accelerators,* Denton, Texas, 1974.
194. Cahill, T. A., *Nucl. Instrum. Methods,* 142, 1 (1977).
195. Barfoot, K. M., Mitchell, I. V., Eschbach, H. L., Mason, P. I., and Gilboy, W. B., *J. Radioanal. Chem.,* 53, 255 (1979).
196. O'Connell, B. and Crumpton, D., *Nucl. Instrum. Methods,* 163, 161 (1979).
197. Neild, D. J., Wise, P. J., and Barnes, D. G., *J. Phys. D,* 5, 2292 (1972).
198. Reuter, F. W. and Smith, H. P. *J. Appl. Phys.* 43, 4228 (1972).
199. Ahlberg, M., *Nucl. Instrum. Methods,* 131, 381 (1975).
200. Kropf, A., *Nucl. Instrum. Methods,* 142, 79 (1977).
201. Benka, O., Geretschläger, M., and Paul, H., *Nucl. Instrum. Methods,* 142, 83 (1977).
202. Végh, J., Berényi, D., Koltay, E., Kiss, I., El-Nasr, S. S., and Sarkadi, L., *Nucl. Instrum. Methods,* 153, 553 (1978).
203. Horowitz, P. and Grodzins, L., *Science,* 189, 795 (1975).
204. Cookson, J. A., Ferguson, A. T. G., and Pilling, F. D., *J. Radioanal. Chem.,* 12, 39 (1972).
205. Nobiling, R., Traxel, K., Bosch, F., Civelekoglu, Y., Martin, B., and Povh, B., *Nucl. Instrum. Methods,* 142, 49 (1977).
206. Brune, D., Lindh, U., and Lorenzen, J., *Nucl. Instrum. Methods,* 142, 51 (1977).

207. **Cookson, J. A.,** *Nucl. Instrum. Methods,* 165, 477 (1979).
208. **Houtman, J. P. W., de Bruin, M., de Goeij, J. J. M., and Tjioe, P. S.,** *Proc. Int Symp. Nucl. Activ. in Life Sciences,* IAEA, Vienna, 1979.
209. **Cookson, J. A., and Pilling, F. D.,** *Phys. Med. Biol.,* 21, 965 (1976).
210. **Legge, G. J. F.,** *Summary of Proc. Aust. Conf. on Nucl. Tech.,* Lucas Heights, 1976, 93.
211. **Horwitz, P., Aronson, M., Grodzins, L., Ladd, W., Ryan, J., Merriam, G., and Lechene, C.,** *Science,* 194, 1162 (1976).
212. **Mazzolini, A. P. J., and Legge, G. J. F.,** *Proc. 2nd Aust. Conf. on Nucl. Tech. of Anal.,* Lucas Heights, 1978, 28.
213. **Legge, G. J. F.,** *Proc. 2nd Aust. Conf. on Nucl. Tech. of Anal.,* Lucas Heights, 1978, 18.
214. **Wilde, H. R., Roth, M., Uhlhorn, C. D., and Gonsior, B.,** *Nucl. Instrum. Methods,* 149, 675 (1978).
215. **Koyama-ito, H., Jahnke, A., Wada, E., Tsumita, T., and Yamazaki, T.,** *Nucl. Instrum. Methods,* 166, 269 (1979).
216. **Fou, C. M., Rasmussen, V. K., Swann, C. P., and Van Patter, D. M.,** *IEEE Trans. Nucl. Sci.,* NS-26, 1378 (1979).
217. **Pierce, T. B., McMillan, J. W., Peck, P. F., and Jones, I. G.,** *Nucl. Instrum. Methods,* 118, 115 (1974).
218. **McMillan, J. W. and Pierce, T. B.,** Nuclear microprobe analysis of reactor materials, in *Ion Beam Surface Layer Analysis, 2,* Meyer, O., Linker, G., and Käppeler, F., Eds., Plenum Press, New York, 1976, 913.
219. **Pierce, T. B. and Huddleston, J.,** *Nucl. Instrum. Methods,* 144, 231 (1977).
220. **McMillan, J. W., Hirst, P. M., Pummery, F. C. W., Huddleston, J., and Pierce, T. B.,** *Nucl. Instrum. Methods,* 149, 83 (1978).
221. **McMillan, J. W., Pummery, F. C. W., Huddleston, J., and Pierce, T. B.,** Quoted in Cookson, J. A., *Nucl. Instrum. Methods,* 165, 477 (1979).
222. **Pierce, T. B.,** *J. Radioanal. Chem.,* 17, 55 (1973).
223. **Clark, G. J., Gulson, B. L., and Cookson, J. A.,** *Summary of Proc. Aust. Conf. on Nucl. Tech.,* Lucas Heights, 1976, 99.
224. **Clark, G. J., Gulson, B. L., and Cookson, J. A.,** *Geochim. Cosmochim. Acta,* 43, 905 (1979).
225. **Gentry, R. V., Cahill, T. A., Fletcher, N. R., Kaufmann, H. C., Medsker, L. R., Nelson, J. W., and Flocchini, R. G.,** *Phys. Rev. Lett.,* 37, 11 (1976).
226. **Cahill, T. A., Fletcher, N. R., Medsker, L. R., Nelson, J. W., Kaufmann, H. C., and Flocchini, R. G.,** *Phys. Rev.,* C17, 1183 (1978).
227. **Cookson, J. A., Fletcher, N. R., Kemper, K. W., Medsker, L. R., and Cahill, T. A.,** Quoted in Cookson, J. A., *Nucl. Instrum. Methods,* 165, 477 (1979).
228. **Bonani, G., Suter, M., Jung, H., Stoller, C., and Wölfli, W.,** *Nucl. Instrum. Methods,* 157, 55 (1978); Wölfli, W., quoted in Cookson, J. A., *Nucl. Instrum. Methods,* 165, 477 (1979).
229. **Suter, M., Bonani, G., Jung, H., Stoller, C., and Wölfli, W.,** *IEEE Trans. Nucl. Sci.,* NS-26, 1373, (1979).
230. **Peisach, M., Newton, D. A., Peck, P. F., and Pierce, T. B.,** *J. Radioanal. Chem.,* 16, 445 (1973).
231. **Allen, C. R., Dearnaley, G., and Hartley, N. E. W.,** Quantitative measurement of light element profiles in thick corrosion films on steels, using the Harwell nuclear micro-beam, in *Ion Beam Surface Layer Analysis, 2,* Meyer, O., Linker, G., and Käppeler, F., Eds., Plenum Press, New York, 1976, 901.
232. **Singleton, J. F. and Hartley, N. E. W.,** *J. Radioanal. Chem.,* 48, 317 (1979).
233. **McKenzie, C.,** quoted in Legge, G. J. F., *Summary of Proc. Aust. Conf. on Nucl. Tech.,* Lucas Heights, 1976, 93.
234. **Umbarger, C. J., Bearse, R. C., Close, D. A., and Malanify, J. J.,** *Adv. X-Ray Anal.,* 16, 102 (1973).
235. **Watson, R. L., Sjurseth, J. R., and Howard, R. W.,** *Nucl. Instrum. Methods,* 93, 69 (1971).
236. **Herman, A. W., McNelles, L. A., and Campbell, J. L.,** *J. Appl. Rad. Isotop.,* 24, 677 (1973).
237. **Bauer, K. G., Fazly, Q., Mayer-Kuckuk, T., Hommsen, H., and Schürkes, P.,** *Nucl. Instrum. Methods,* 148, 407 (1978).
238. **Gilfrich, J. V., Burkhalter, P. G., and Birks, L. S.,** *Anal. Chem., 45, 2002 (1973).*
239. **Goulding, F. S. and Jaklevic, J. M.,** *Nucl. Instrum. Methods,* 142, 323 (1977).
240. **Scheer, J., Voet, L., Wätjen U., Koenig, W., Richter, F. W., and Steiner, U.,** *Nucl. Instrum. Methods,* 142, 333 (1977).
241. **Moriya, Y., Ato, Y., and Miyagawa, S.,** *Nucl. Instrum. Methods,* 150, 523 (1978).
242. **Cairns, J. A., Holloway, D. F., and Nelson, R. S.,** *Adv. X-Ray Anal.,* 14, 173 (1971).
243. **Gryzinski, M.,** *Phys. Rev.,* 138, A336 (1965).